8508 J. Med. Chem. 2010, 53, 8508–8522
DOI: 10.1021/jm100732t

Journal of Medicinal Chemistry Article

A Novel Pyrazolo[1,5-*a*]pyrimidine Is a Potent Inhibitor of Cyclin-Dependent Protein Kinases 1, 2, and 9, Which Demonstrates Antitumor Effects in Human Tumor Xenografts Following Oral Administration

Dean A. Heathcote,[†] Hetal Patel,[†] Sebastian H. B. Kroll,[‡] Pascale Hazel,[§] Manikandan Periyasamy,[†] Mary Alikian,[†] Seshu K. Kanneganti,[†] Ashutosh S. Jogalekar,[∥] Bodo Scheiper,[‡] Marion Barbazanges,[‡] Andreas Blum,[‡] Jan Brackow,[‡] Alekasandra Siwicka,[‡] Robert D. M. Pace,[‡] Matthew J. Fuchter,[‡] James P. Snyder,[∥] Dennis C. Liotta,[∥] Paul. S. Freemont,[§] Eric O. Aboagye,[†] R. Charles Coombes,[†] Anthony G. M. Barrett,[‡] and Simak Ali*[,†]

[†]*Dept of Oncology, Imperial College London, Hammersmith Hospital Campus, Du Cane Road, London W12 0NN, England,* [‡]*Department of Chemistry, Imperial College London, London SW7 2AZ, England,* [§]*Division of Molecular Biosciences, Imperial College London, London SW7 2AZ, England, and* [∥]*Department of Chemistry, Emory University, Atlanta GA30322, United States*

Received June 17, 2010

Cyclin-dependent protein kinases (CDKs) are central to the appropriate regulation of cell proliferation, apoptosis, and gene expression. Abnormalities in CDK activity and regulation are common features of cancer, making CDK family members attractive targets for the development of anticancer drugs. Here, we report the identification of a pyrazolo[1,5-*a*]pyrimidine derived compound, **4k** (BS-194), as a selective and potent CDK inhibitor, which inhibits CDK2, CDK1, CDK5, CDK7, and CDK9 (IC_{50} = 3, 30, 30, 250, and 90 nmol/L, respectively). Cell-based studies showed inhibition of the phosphorylation of CDK substrates, Rb and the RNA polymerase II C-terminal domain, down-regulation of cyclins A, E, and D1, and cell cycle block in the S and G_2/M phases. Consistent with these findings, **4k** demonstrated potent antiproliferative activity in 60 cancer cell lines tested (mean GI_{50} = 280 nmol/L). Pharmacokinetic studies showed that **4k** is orally bioavailable, with an elimination half-life of 178 min following oral dosing in mice. When administered at a concentration of 25 mg/kg orally, **4k** inhibited human tumor xenografts and suppressed CDK substrate phosphorylation. These findings identify **4k** as a novel, potent CDK selective inhibitor with potential for oral delivery in cancer patients.

Introduction

Cyclin-dependent kinases (CDK[a]) are serine/threonine kinases that regulate progression through the cell cycle. CDK4 and CDK6 mediate progression through the G_1 growth phase, CDK2 is required for entry into and transition through the DNA replication or synthesis (S) phase, and CDK1 controls progression through G_2 and mitosis. CDK7, together with its partners cyclin H and MAT1, form the CDK activating kinase (CAK), which activates the cell cycle CDKs by phosphorylating them at a threonine residue in the activation segment (T-loop).[1−3]

Deregulation of cell cycle progression is a universal characteristic of cancer, and the majority of human cancers have abnormalities in some component of CDK activity, frequently through elevated and/or inappropriate CDK activation. Examples include cyclin overexpression, for example, cyclin D1 overexpression is commonly observed in breast cancer,[4] and loss of expression of CDK inhibitory proteins (CKI) through mutational or epigenetic alterations, for example, p16 loss has been observed in skin, lung, breast, and colorectal cancer (for review see ref 5). Synthetic inhibitors of CDK activity therefore present as a logical approach in the development of new cancer therapies. However, the development of inhibitors selective for a particular CDK has been questioned by the finding that inhibition of some CDKs may lead to compensation by other CDKs. For example, cells from mice that have been ablated for CDK2 are able to cycle, and $CDK2^{-/-}$ mice are viable,[6,7] while evidence for compensation of CDK2 by CDK1 has been forthcoming.[8,9] Similarly, $CDK4^{-/-}$ and $CDK6^{-/-}$ mice are viable, although the double null mice show late embryonic lethality.[10−12] Hence, a highly selective inhibitor of CDK2, 4, or 6 may be subject to clinical resistance due to the potential for compensation. However, acquisition of CDK dependence seems to feature in some tumor types. For example, despite the fact that CDK4 is not required for normal mammary gland development, it does appear to be important for induction of mammary tumors in mouse models.[13−15] The CDK4/CDK6 partner cyclin D1 is similarly required for HER2- and Ras-induced mammary tumors, but not for Myc and Wnt1 induced mammary tumors,[16] indicating that, at least in some tumor types, requirement for selective CDKs is acquired during the process of tumorigenesis in a process that is dependent on the pathway leading to tumor formation.[3,17]

*To whom correspondence should be addressed. Phone: +44 20 8383 3789. Fax: +44 20 8383 5830. E-mail: simak.ali@imperial.ac.uk.

[a] Abbreviations: CDK, cyclin dependent kinase; Rb, retinoblastoma; PolII, RNA polymerase II; CKI, CDK inhibitory protein; HUVEC, human normal vascular endothelial cells; PBMC, peripheral blood mononuclear cells; SRB, sulforhodamine B; FACS, fluorescence-activated cell sorter, ADME-Tox, absorption, distribution, metabolism, excretion, and toxicity; PO, per oral, IV, intravenous; IP, intraperitoneal.

 Published on Web 11/16/2010

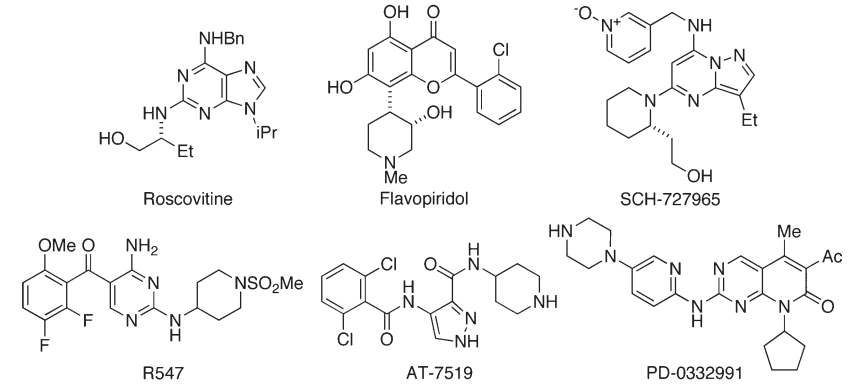

Figure 1. Structures of some CDK inhibitors currently in clinical evaluation. See text for references.

Scheme 1. Synthesis of Pyrazolopyrimidines[a]

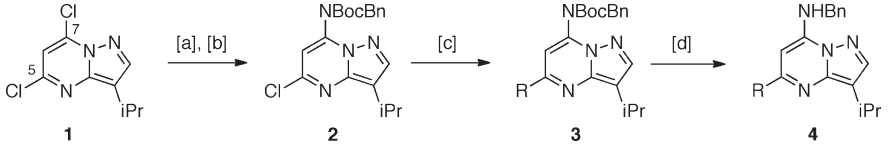

[a] (a) $BnNH_2$, EtOH, reflux, 16 h, 95%; (b) Boc_2O, THF, cat. DMAP, 25 °C, 20 h, 96%; (c) amine, $Pd_2(dba)_3$, *rac*-BINAP, NaO^tBu, 100 °C, 16 h, 40−99%; (d) MeOH, HCl, 25 °C, 3 h, 67−99%.

We reasoned that inhibitors of CDK7 could be potentially important in cancer therapy, as they would inhibit activation of many of the cyclin-dependent kinases involved in cell cycle progression. Moreover, as part of the TFIIH general transcription factor complex, CDK7/CycH/MAT1 mediates the phosphorylation of the C-terminal domain of the largest subunit of RNA polymerase II, an event required for promoter clearance and transcription initiation.[18−20] In carrying out a screen for CDK7 inhibitors, we identified a compound, **4k**, which inhibits CDK7 but is also a potent inhibitor of CDK1, CDK2, CDK5, and CDK9. In further evaluating the activity of **4k**, we show that **4k** potently inhibits growth of the great majority of cancer cell lines examined and inhibits phosphorylation of CDK substrates at submicromolar concentrations. A number of inhibitors that target cell cycle CDKs have been identified and some have been evaluated clinically, including roscovitine (Seliciclib), SCH-727965, and AT7519 (Figure 1).[21−23] **4k** is a pyrazolopyrimidine as is SCH-727965. Unlike many other CDK inhibitors, however, we show that **4k** is orally bioavailable and inhibits tumor growth in vivo. As such, **4k** is an important new CDK inhibitor with clinical potential.

Results

Identification of 4k. Of the CDK inhibitors currently undergoing clinical trials (Figure 1), a structural class that has yielded several CDK-selective ATP antagonists is the 2,6,9-trisubstituted purines, exemplified by roscovitine, which shows good biological and pharmacological properties. However, our computational analysis has shown that the pyrazolo[1,5-*a*]pyrimidine core has a less favorable aqueous solvation energy than the corresponding purine, suggesting that this compound class would be more readily transferred into the hydrophobic kinase active site.[24,25] In this study, a range of pyrazolopyrimidines were synthesized and tested for CDK activity.

The compounds were readily accessible from dichloropyrazolo[1,5-*a*]pyrimidine **1** by sequential selective substitution of the C-7 chloride using benzylamine followed by palladium-catalyzed displacement of the C-5 chloride under Buchwald−Hartwig reaction conditions, as described previously (Scheme 1).[24] Protection of the benzylic amine as a carbamate was essential for successful C-5 amination. Following deprotection, the analogues were assayed for CDK activity by measurement of free ATP remaining in the kinase reaction, as determined using a luciferase assay.

The high potency offered by the pyrazolopyrimidine core was highlighted by the effective inhibition of several CDKs by **4a**, which bears the roscovitine side chain (Supporting Information Table 1). Deletion of the free hydroxyl group in **4b** had a large detrimental effect on the potency. Interestingly, chain elongation and replacement of the hydroxyl by a terminal amine **4c** selectively increases potency toward CDK7. Compound **4c**, which we have previously reported (BS-181), inhibits CDK7 activity up to 83% while demonstrating only weak inhibition of the other CDKs. Compound **4c** inhibited CDK7 activity, with an IC_{50} of 21 nm/L, with greater than 40-fold selectivity over other CDKs and a wider range of 70 kinases and additionally showed antitumor activity in vivo.[24]

Further long chain C-5 analogues were synthesized, and nitrile **4d** showed a similar inhibition of CDK7 activity (IC_{50} 20 nm/L) while also showing increased CDK2 inhibition. Similarly, amidine **4e** showed only a slight decrease in CDK7 inhibition (IC_{50} 40 nm/L), however, this also proved to be a highly potent CDK2 inhibitor.

Having identified **4c** as a potent and selective CDK7 inhibitor, it was decided to further investigate the SAR around the C-5 side chain against CDK potency and selectivity. Several analogues containing a terminal basic residue in combination with a free hydroxyl group were investigated. These were readily synthesized from alkene **6** (see Scheme 2) via cross metathesis, or oxidation/Wittig reactions followed by reduction of the resultant alkene prior to Buchwald−Hartwig coupling. However, the parent alkene **4f** showed decreased inhibition compared to the analogue with the roscovitine side chain **4a**,

Scheme 2. First Generation Synthesis of 4k and 4l[a]

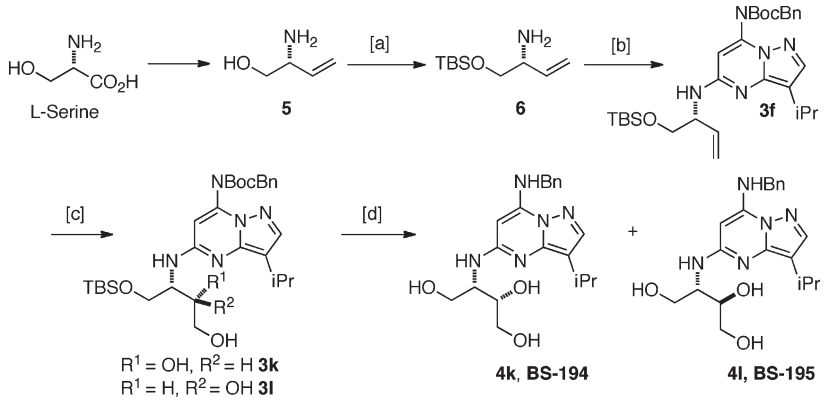

[a] (a) *t*-BuMe$_2$SiCl, Et$_3$N, cat. DMAP, CH$_2$Cl$_2$, 25 °C, 16 h, 99%; (b) **2**, Pd$_2$(dba)$_3$, *rac*-BINAP, NaO^{t}Bu, 100 °C, 16 h, 43%; (c) cat. OsO$_4$, NMO, MeCN, H$_2$O, 25 °C, 45 min, **3k** 42%, **3l** 33%; (d) MeOH, HCl, 25 °C, 3 h, **4k** 79%, **4l** 67%.

Table 1. Inhibition of Cyclin-Dependent Protein Kinase Activity by **4k**[a]

kinase	roscovitine IC_{50} (μM) (SD)	**4k** IC_{50} (μM) (SD)
CDK1	2.1 (0.5)	0.033 (0.01)
CDK2	0.1 (0.05)	0.003 (0.001)
CDK4	13.5 (0.2)	20 (1.3)
CDK5	0.16 (0.2)	0.03 (0.006)
CDK6	23.5 (1.3)	35.5 (1.3)
CDK7	0.54 (0.09)	0.25 (0.04)
CDK9	0.95 (0.17)	0.09 (0.01)

[a] The mean IC_{50} values (μM) for roscovitine and **4k**, obtained from three experiments, are shown, together with the standard deviation (SD) from the mean. The line graphs from which IC_{50} values were obtained are shown in Supporting Information Figure 1.

and none of the analogues with the functionalized side chains **4g**, **4h**, or **4i** showed any significant inhibition of the CDKs.

The importance of free hydroxyl groups however, was reinforced by the high CDK7 inhibition and good selectivity demonstrated by the 2-(2-hydroxyethoxy)-ethylamino analogue **4j**. Accordingly, further hydroxylated compounds were synthesized by dihydroxylation of the vinyl residue present in **3f**, which after diastereoisomer separation and deprotection yielded the two amino triols **4k** and **4l** (BS-195). Both diastereoisomers proved to be highly active against a range of CDKs.

4k was chosen for further study because it inhibited CDK2 with an IC_{50} = 3 nmol/L (Table 1; Supporting Information Figure 1), an IC_{50} more than 30-fold lower than that showed by roscovitine (IC_{50} = 100 nmol/L).[26] **4k** also inhibited CDK1 (IC_{50} = 33 nmol/L), CDK5 (IC_{50} = 30 nmol/L), and CDK9 (IC_{50} = 90 nmol/L) and was a less potent inhibitor of CDK7 (IC_{50} = 250 nmol/L), whereas CDK4 and CDK6 were not inhibited by **4k**. Compound **4l** gave a similar profile of CDK inhibition, however, **4k** had the advantage of being a crystalline solid. Compound **4k** was therefore selected for development due to both potency and ease of purification. In addition, the relative configuration of the molecule and by analogy its absolute stereochemistry was readily assigned by an X-ray crystal structure determination (Figure 2).

The initial synthesis of **4k** using a nonselective late stage alkene dihydroxylation reaction usefully gave access to both diastereoisomers, however, the diastereoisomer separation was laborious and unsuitable once **4k** had been selected for development (Scheme 2). Accordingly, an alterative route to

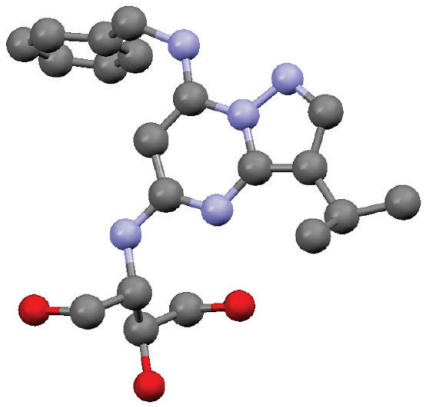

Figure 2. Crystal structure of **4k**.

enantiomerically and diastereomerically pure **4k** was investigated. We decided to introduce a fully functionalized C-5 side chain through the existing Buchwald−Hartwig coupling reaction, therefore a synthesis of the requisite fully protected amino-triol was required.

(−)-Diethyl tartrate (**8**) was converted to the corresponding cyclic sulfate using reaction conditions developed by Sharpless, by conversion to the cyclic sulfite with thionyl chloride, followed by ruthenium catalyzed oxidation to the cyclic sulfate.[27] Subsequent ring S$_N$2 opening using sodium azide gave the requisite azido-alcohol **9**. However, the oxidation reaction proved to be capricious, and as a consequence of difficulties encountered with handling of the cyclic sulfate, a more reliable method was investigated. Direct S$_N$2 ring-opening of the cyclic sulfite with sodium azide with careful control of temperature was highly effective, giving azide **9** in 70% yield.[28] The diester was readily reduced to triol **10** by lithium borohydride generated in situ in EtOH.[28,29] It was necessary to protect the free hydroxyl groups to prevent competitive *O*-arylation in the Buchwald−Hartwig coupling, and it was hoped to achieve this in a single operation. However, attempts to protect all the hydroxyl groups as an orthoester by condensation with trimethyl orthoacetate or trimethyl orthobenzoate with acid catalysis failed. Attempts to prepare the triple methoxymethyl ether were complicated by formation of cyclic acetals and were only low yielding. A two-step procedure was therefore employed with the vicinal diol first being protected as an acetonide and the primary alcohol subsequently protected by methoxymethylation.

Scheme 3. Second Generation Synthesis of 4k[a]

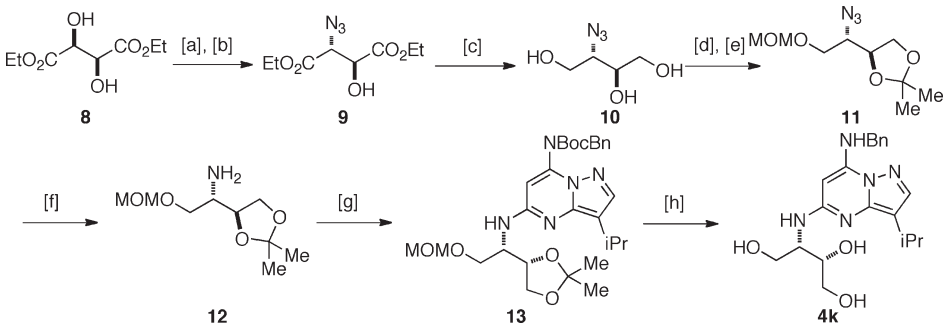

[a] (a) $SOCl_2$, NEt_3, CH_2Cl_2, 0 °C, 1 h; (b) NaN_3, DMF, 12 h, 70% (2 steps); (c) $NaBH_4$,LiCl, EtOH, 0 °C, 12 h; (d) $(MeO)_2CMe_2$, TsOH, Me_2CO, 50 °C, 3 h; (e) MOMCl,*i*Pr_2NEt, CH_2Cl_2, 0 °C, 12 h, 70% (3 steps); (f) H_2, Pd/C, MeOH, 1 h, 97%; (g) **2**,$Pd_2(dba)_3$, *rac*-BINAP, NaO^{t}Bu, 100 °C, 16 h, 95%; (h) MeOH, HCl, 25 °C, 3 h, 90%.

Catalytic hydrogenation over palladium on charcoal gave the required fully protected amine **12**, which underwent high yielding Buchwald−Hartwig coupling to produce the protected **4k** precursor **13**. Global deprotection under acidic conditions gave **4k** as a single stereoisomer (Scheme 3). The ^{1}H and ^{13}C NMR spectra of **4k** are shown in Supporting Information Figures 2 and 3.

4k Is a Potent Inhibitor of CDK1, CDK2, CDK7, and CDK9. Determination of the CDK selectivity of **4k**, performed by assaying inhibition of the activities of 76 proteins kinases representing members of different kinase classes (Table 2), showed significant inhibition of CAMKKβ, CK1, DYRK1A, ERK1, ERK2, and IRR at 10000 nmol/L but a less than 50% inhibition of these kinases when **4k** was used at a concentration of 1000 nmol/L (data not shown), suggestive of IC_{50} values >1000 nmol/L. In confirmation of this, the IC_{50} values for CAMKKβ, CK1, DYRK1A, ERK1, ERK2, and IRR were determined as 2450, 1040, 2100, 3730, 3110, and 1800 nmol/L, respectively. The only exception was ERK8, whose activity was inhibited by 74% with 10 μmol/L **4k** and the IC_{50} was determined as 330 nmol/L (data not shown), 100-fold higher than the IC_{50} for CDK2, about 10-fold higher IC_{50} than that obtained for CDK1 or CDK5.

A 1.8 Å crystal structure of **4k** bound to the inactive form of CDK2 was obtained by soaking the ligand into preformed CDK2 crystals. After molecular replacement with the published CDK2 structure, clear and unambiguous density for the ligand was found within the CDK2 ATP binding site (Figure 3A,D). Compound **4k** binds in a similar fashion to roscovitine, with the core heterocyclic ring occupying approximately the same position as the ATP purine ring.[30] The phenyl ring substituent occupies a hydrophobic pocket outside the ATP binding site, while N1 and N6 each form a hydrogen bond to the L83 main chain, as seen in the structure of roscovitine bound to CDK2 (Figure 3B,C). In addition, the three side chain hydroxyl groups of **4k** form several water-mediated interactions with CDK2 backbone and side chain atoms, involving residues E12, T14. D86, Q131, and D145 (Figure 3B). This is in contrast to roscovitine, where the number of stabilizing water-mediating interactions between the single ligand hydroxyl group and CDK2 is limited (Figure 3C). The structure suggests that the increased potency of **4k** in CDK2 inhibition assays compared to roscovitine could be due to tighter binding of the former to the inactive state of CDK2. The increased affinity of **4k** compared to roscovitine stems from its ability to form a network of water mediated interactions within the CDK2 ATP binding pocket. Due to a major movement of the glycine loop (residues 12−20) upon cyclin binding to CDK2, it is expected that the **4k** hydroxyl substituents will form different interactions

Table 2. Inhibition of Protein Kinases by **4k**[a]

4k (10 μM)			**4k** (10 μM)		
enzyme	% activity remaining	SD	enzyme	% activity remaining	SD
MKK1	65	15	AMPK	88	1
ERK1	42	15	MARK3	82	4
ERK2	26	4	BRSK2	108	14
JNK1	93	3	MELK	88	1
JNK2	94	12	CK1	19	1
p38a MAPK	98	12	CK2	89	7
P38b MAPK	94	3	DYRK1A	15	3
p38g MAPK	112	14	DYRK2	75	1
p38s MAPK	86	0	DYRK3	88	1
ERK8	26	4	NEK2a	102	3
RSK1	75	15	NEK6	87	15
RSK2	90	1	IKKb	80	3
PDK1	84	11	PIM1	103	6
PKBa	103	6	PIM2	94	1
PKBb	105	9	PIM3	101	5
SGK1	92	1	SRPK1	62	14
S6K1	77	0	MST2	86	8
PKA	93	2	EFK2	92	1
ROCK 2	102	14	HIPK2	73	6
PRK2	106	3	PAK4	55	7
PKCa	96	4	PAK5	65	3
PKC ζ	64	14	PAK6	85	6
PKD1	97	15	Src	95	13
MSK1	96	1	Lck	85	2
MNK1	98	3	CSK	77	1
MNK2	136	15	FGF-R1	86	2
MAPKAP-K2	111	14	IRR	32	11
PRAK	97	8	EPH A2	116	10
CAMKKb	23	1	MST4	92	14
CAMK1	93	5	SYK	120	11
SmMLCK	101	13	YES1	89	7
PHK	62	8	IKKe	94	7
CHK1	98	8	TBK1	87	8
CHK2	61	5	IGF1-R	67	15
GSK3b	63	15	VEG-FR	92	8
CDK2-cyclin A	3	0	BTK	91	8
PLK1	68	4	IR-HIS	70	2
PLK1 (okadaic acid)	97	14	EPH-B3	72	13

[a] Inhibition of 76 protein kinases by **4k** at a concentration of 10 μmol/L. The assay was carried out in duplicate. Percentage of kinase activity remaining is shown, together with the standard deviations (SD).

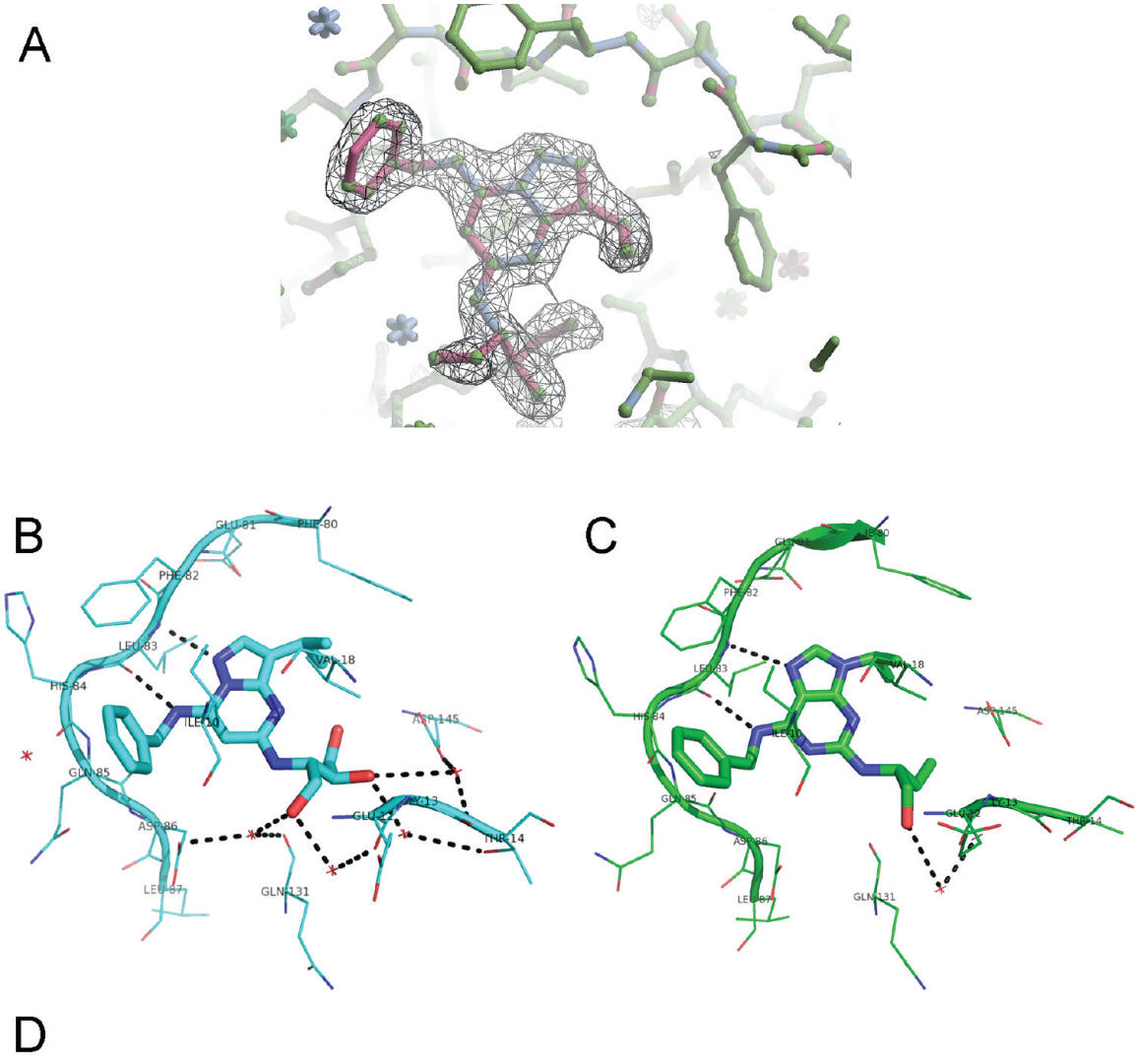

Space group and unit cell (Å)	$P2_12_12_1$, a = 53.05, b = 70.69, c = 72.11
Resolution range (Å) (last shell)	42.73-1.78 (1.88-1.78)
R_{merge}	0.095 (0.699)
Observations	87242 (12389)
Unique observations	26364 (3774)
Mean(I)/σ(I)	6.7 (1.7)
Completeness	99.4 % (99.6 %)
Multiplicity	3.3 (3.3)
Refinement statistics	
R_{factor}	0.201
R_{free}	0.266
Rmsd bond lengths (Å)	0.025
Rmsd bond angles (°)	2.023

Figure 3. Crystal structure of **4k** bound to CDK2. (A) Shown is the **4k** difference electron density map after refinement, contored at 2.9σ. (B) **4k** binding site in CDK2 is shown with hydrogen bonding interactions depicted as dashed lines. Water-mediated interactions are also shown. Carbon atoms are colored in cyan, nitrogen in blue, and oxygen in red. Water molecules are represented as red crosses. (C) Roscovitine binding site in CDK2 (PDB code 2A4L), as (B). (D) Summary of CDK2-**4k** data collection and refinement statistics.

in the active complex, and we are currently progressing studies to obtain a structure for **4k** bound to the active CDK2-cyclin A complex. Notwithstanding, the crystallography data confirm **4k** structure and binding to CDK2.

4k Promotes Cell Cycle Arrest and Inhibits Cancer Cell Growth. A panel of cell lines representing a range of tumor types, including breast, lung, prostate, and colorectal cancer, were treated with increasing concentrations of **4k** for 72 h.

Table 3. In Vitro Growth Inhibitory Activity of **4k**[a]

cell type	cell line	roscovitine GI_{50} (μM) (SD)	**4k** GI_{50} (μM) (SD)
breast	MCF-7	7.8 (0.2)	0.3 (0.1)
	MDA-MB-231	22.6 (0.1)	0.3 (0.1)
	MCF-10A	16.3 (0.1)	0.1 (0.1)
colorectal	COLO-205	24.9 (0.2)	0.12 (0.1)
	HCT-116	15.5 (0.1)	0.1 (0.1)
lung	A549	15 (0.2)	0.2 (0.1)
osteosarcoma	SaOS2	13.9 (0.1)	0.25 (0.1)
prostate	PC3	25.2 (0.1)	0.5 (0.1)
liver	HepG2	25.9 (0.2)	1.0 (0.1)
ovarian	Sk-Ov-3	35.7 (0.2)	0.3 (0.2)
human normal umbilical vein endothelial cells (HUVEC)		3.7 (0.1)	6.3 (0.1)

[a] The mean IC_{50} values (μM) were obtained using the sulforhodamine B (SRB) assay. Shown are the mean values derived from at least three replicates, together with the standard deviations (SD) from the means.

Determination of proliferation using the sulforhodamine B (SRB) assay showed that growth was inhibited for all cell lines tested, with 50% growth inhibition (GI_{50}) values of 100−500 nmol/L (Table 3). By contrast, GI_{50} values for roscovitine ranged between 7.8−35.7 μmol/L for the same cell lines. Interestingly, human normal vascular endothelial cells (HUVEC) (GI_{50} = 6.3 μmol/L) were somewhat less sensitive to **4k** than the cancer lines.

On the basis of our findings, **4k** was submitted to the Developmental Therapeutics Program at the NCI (http://dtp.nci.nih.gov) for testing using the NCI60 cancer cell line screen. In this screen, treatment with **4k** showed potent inhibition of all 60 cancer lines (Figure 4A, Supporting Information Figure 4), with $GI_{50} < 1$ μmol/L (mean $GI_{50} = 2.81 \times 10^{-7}$ mol/L). For the great majority of the lines, the 50% lethal concentration (LC_{50}) was >100 μmol/L (mean $LC_{50} > 10 \times 10^{-4}$ mol/L) (Supporting Information Table 2). For comparison, in the same cell panel, flavopiridol is a potent inhibitor of cancer cell growth (mean $GI_{50} = 7.47 \times 10^{-8}$ mol/L) but lethal concentration for flavopiridol is reached at submicromolar concentrations ($LC_{50} = 9.04 \times 10^{-7}$ mol/L) (http://dtp.nci.nih.gov).

Flow cytometric analysis of HCT116 cells treated with 1 and 10 μmol/L **4k** showed a significant reduction in cells in G1, with a concomitant increase in cells in S and G2/M phases of the cell cycle (Figure 4B; Supporting Information Figure 5), as would be expected from the potent inhibition of CDK1 and CDK2, but not of CDK4 and CDK6, by **4k**. Similar effects were observed in MCF-7 cells (data not shown). There was also an increase in the sub-G1 population, suggestive of a small, but significant amount of apoptosis at 1 and 10 μmol/L **4k**, which was confirmed by annexin V staining (data not shown).

4k Inhibits Phosphorylation of CDK Substrates and Promotes Loss of Cyclin Expression. Immunoblotting of whole cell lysates prepared from HCT116 colon cancer cells treated with **4k** for 4 and 24 h showed inhibition of the phosphorylation of the CDK2 substrate RB at Ser-780, Ser-795, Ser-801, Ser-807/Ser-811, and Thr-821 (Figure 4C,D), the CDK1 substrate protein phosphatase type 1α (PP1a) at Thr-320, and the CDK9 substrate Ser-2 in the C-terminal domain (CTD) of RNA polymerase II (PolII). Altered levels of CDKs or cyclins did not accompany inhibition of RB and PolII phosphorylation at 4 h following **4k** addition (Figure 4E). By contrast, at 24 h, levels of cyclin A, cyclin B, and cyclin D1 were dramatically reduced in the case of **4k** at a concentration of 1 μmol/L. Reduction in the levels of these cyclins was also observed with higher concentrations (30 and 40 μmol/L) of roscovitine. CDK2 levels were not influenced by **4k** treatment, although its levels were reduced at high concentrations of roscovitine. Phosphorylation of Thr-170 of CDK2 was, however, reduced following 24 h treatment with **4k**. Together, these results indicate a rapid inhibition of CDK activity following **4k** addition, with slower acting effects on cyclin levels.

In Vivo Pharmacokinetic Studies and Tumor Growth Inhibition. To determine whether **4k** inhibits tumor growth in vivo, nude mice bearing MCF-7 tumors were injected intraperitoneally twice daily with 5 or 10 mg/kg, to give total daily doses of 10 mg/kg or 20 mg/kg, over a period of 14 days. Tumor growth was inhibited in a dose-dependent manner, with 30% and 40% reduction in tumor growth, compared with the control group, for 10 and 20 mg/kg/day doses of **4k**, respectively (Figure 5A). At these doses, there was no apparent toxicity, as judged by lack of significant adverse effects on animal weights (Figure 5B).

Compound **4k** was found to have favorable absorption, distribution, metabolism, elimination, and toxicity (ADME-Tox) properties. The drug had an aqueous solubility (PBS, pH 7.4) of 54.0 μmol/L (range, 47.16−60.89 μmol/L) and partition coefficient (Log *D*, *n*-octanol: PBS pH 7.4) of 3.0. In vitro cellular absorption (A−B permeability, TC7, pH 6.5/7.4) of **4k** was 9.7×10^{-6} cm·s^{-1} (range, $9.32-10.06 \times 10^{-6}$ cm·s^{-1}; recovery = 91±%) at a test concentration of 10 μmol/L. In the same assay, the absorption of propranolol used as control was 54.2×10^{-6} cm·s^{-1} (range, $53.64-54.81 \times 10^{-6}$ cm·s^{-1}; recovery = 85±%). Whereas plasma protein binding did not differ significantly between mouse and human, microsomal metabolism was found to be more favorable for human compared to mouse liver microsomes (Table 4). Injection of **4k** at 10 mg/kg into mice via the intraperitoneal (IP), intravenous (IV), and oral (PO) routes of administration of resulted in terminal elimination half-lives of 147, 210, and 178 min, respectively, with the measured plasma concentration at 15 min of 10474 (SEM = 5634), 25351 (SEM = 780), and 9347 (SEM = 551) ng/mL, respectively (Table 5; Figure 6). One of two metabolites detected after intravenous administration of **4k** was identified as an oxidative (hydroxylated) metabolite (data not shown).

Pharmacokinetic studies indicated good oral bioavailability (88%; n = 3 animals for 8 time points analyzed for each of PO and IV administration) for **4k**. To determine whether treatment with **4k** elicits responses in vivo, **4k** was administered by oral gavage to nu/nu-BALB/c athymic nude mice. Immunostaining and flow cytometric analysis of peripheral blood mononuclear cells (PBMC) isolated 6 h following administration showed that **4k** at concentrations of 25 mg/mL induced a 60−70% reduction in RB phosphorylation at Thr-821 (Figure 7). There were also 25−50% fall in PolII Ser-2 and Ser-5 phosphorylation with 25 mg/mL **4k**, with reductions in phosphorylation of PolII being maximal at 100 mg/mL **4k**, although at concentrations of 50 mg/mL or higher, PolII levels also fell. No difference in RB Thr-821 or PolII phosphorylation was evident 24 h following administration with 50 mg/mL **4k**, although RB Thr-821 phosphorylation was reduced by 50% ($p < 0.01$), 24 h after administration of 75 mg/mL **4k** (data not shown).

The above results indicated that oral administration of **4k** results in rapid down-regulation of RB and PolII phosphorylation

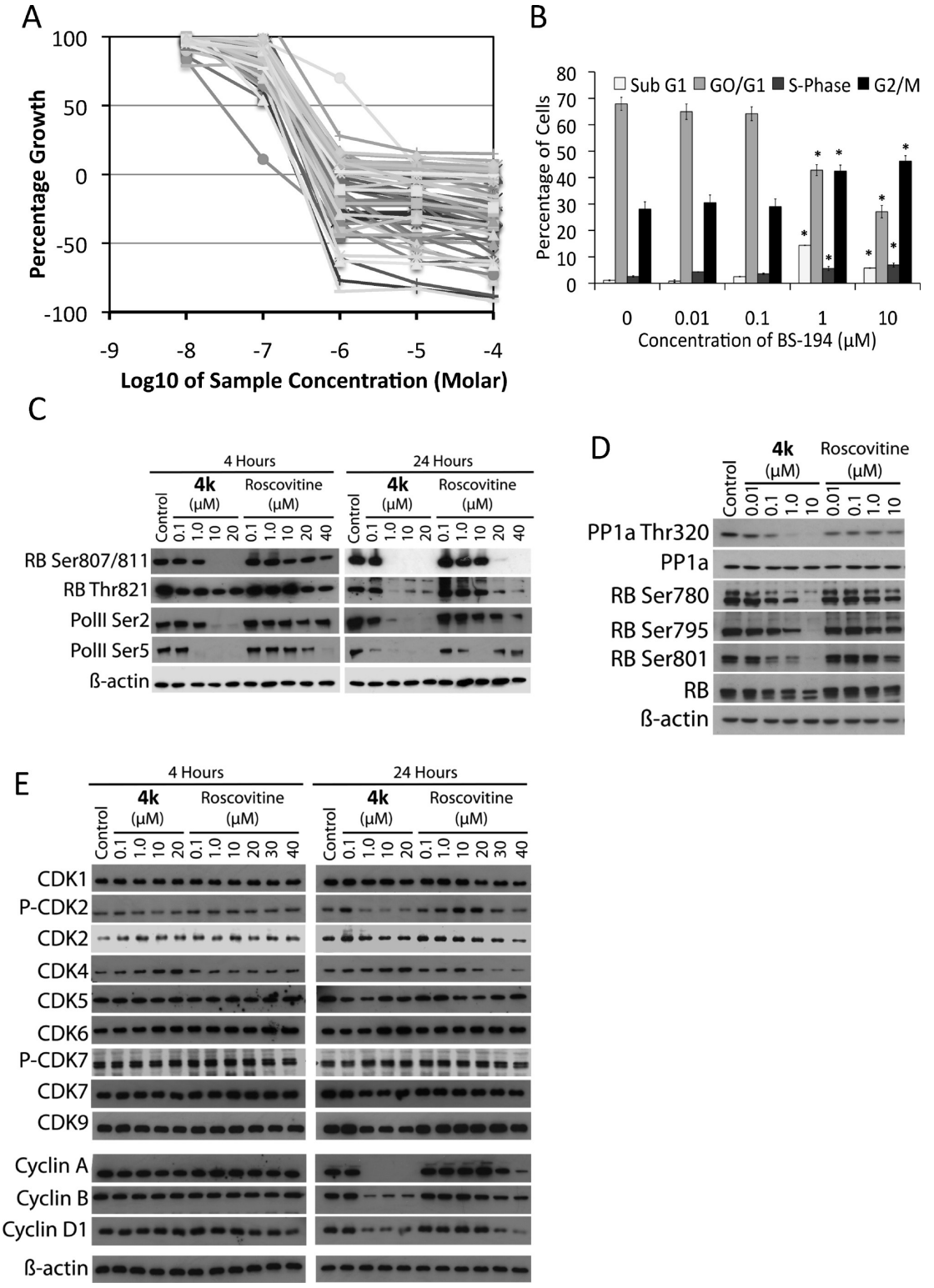

Figure 4. Compound **4k** treatment of HCT116 cells leads to cancer cell growth inhibition, cell cycle arrest, and inhibition of CDK substrate phosphorylation. (A) Growth inhibition profiles for the NCI 60 cancer cell panel. For details of the growth profiles of the individual cell lines see Supporting Information. (B) Effect of **4k** on cell cycle kinetics. **4k** at the concentrations shown was added to HCT116 cells for 24 h prior to fixation, staining with propidium iodide (PI), and flow cytometric analysis. The percentage of cells in the sub-G1 (apoptosis), G1, S-phase, and G2/M, as determined from three independent experiments, are shown. Error bars represent the standard errors of the mean (SEM). *P*-Values were determined using Student's *t* test, in which comparison between the DMSO control, and **4k** treatment at each concentration was carried out. Asterisks (*) denote $p < 0.05$. (C−E) Molecular pharmacology of **4k** on HCT116 cells. Cell lysates prepared from HCT116 cells treated with **4k** or roscovitine for 4 or 24 h were immunoblotted for various proteins or phosphorylated forms, as labeled.

but recovery within 24 h. To determine if oral administration of **4k** inhibits the growth of HCT116 tumor xenografts, animals were treated once daily with 25 mg/kg **4k** by oral gavage. Tumor growth was inhibited in a dose-dependent manner, with

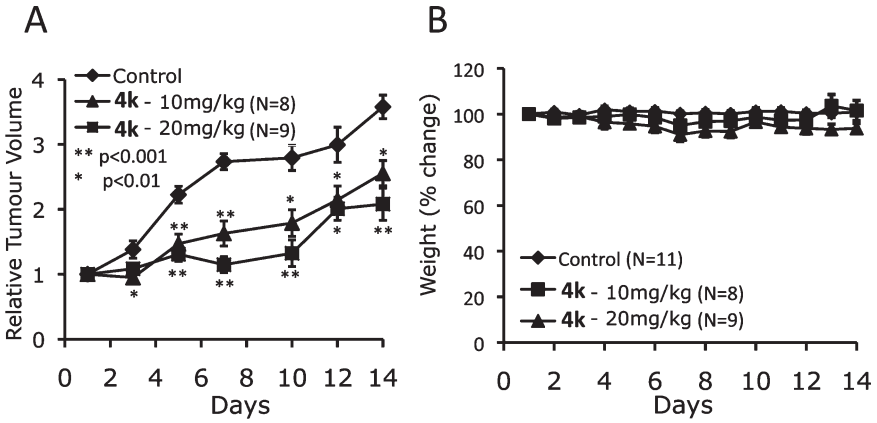

Figure 5. Compound **4k** inhibits growth in human breast tumor xenografts. (A) Randomized MCF-7 tumor bearing mice were injected intraperitoneally twice daily with vehicle (control, $n = 11$) or with 5 or 10 mg/kg of **4k**, giving a total daily dose of 10 mg/kg/day ($n = 8$) or 20 mg/kg/day ($n = 9$), respectively, over a period of 14 days. The change in tumor volume was determined for each animal, as tumor volume relative to the tumor volume of each animal at day 1. The line graphs show the mean tumor volumes for the animals in each treatment group. (B) Shown are the weights of the animals used over the time course of the study. Error bars represent the standard errors of the mean.

Table 4. In Vitro Plasma Protein Binding and Microsomal Metabolism of **4k**[a]

plasma protein binding		
test concentration, μM	% protein bound (human)	% protein bound (mouse)
4k, 10	94.3 (94.0 −94.5)	88.3 (86.0−90.6)
quinidine, 10	71.1 (65.3−76.9)	71.1 (70.0−72.2)
in vitro metabolism (metabolic stability) (liver microsomes)		
test concentration, μM	parent remaining (human) (%)	parent remaining (human) (%)
4k, 1.0	83 (80.6−84.8)	29 (28.8−29.1)
propranolol, 1.0	74 (73.5−75.2)	37 (34.7−39.6)

[a] Data are mean values (range). Incubation: 0 and 60 min at 37 °C. Substrate/co-factor: test compound (1 μM), NADP (1 mM), G6P (5 mM), G6PDHase (1 U/mL) with 0.6% methanol, 0.6% acetonitrile ($n = 2$).

50% reduction in tumor growth in the 25 mg/kg/day group (Figure 8A), with no significant loss in animal weights in the vehicle or **4k** treatment groups. (Figure 8B).

Immunohistochemical staining of resected tumors showed no difference in Rb level in the vehicle or **4k** treatment groups (Figure 8C,D). By contrast. levels of Rb phosphorylation at Ser807/811 and Thr821 were decreased in the **4k** treated tumors when compared with the vehicle treated group ($p < 0.005$).

Discussion

Recent studies show that inhibition of individual CDKs required for cell cycle progression may be ineffective cancer treatments either because they are not essential or due to potential compensation by other CDKs.[3] For example, in the case of CDK2, a popular target for drug discovery due to its role in progression through the S phase, inhibition of this kinase was insufficient to prevent cancer cell proliferation,[31] whereas combined depletion of CDK2 and CDK1 in cancer cells resulted in greater cell cycle arrest than seen with depletion of CDK2 or CDK1 alone.[9] In this context, the potent CDK1 and CDK2 inhibitory activity of **4k** provides an attractive therapeutic approach. Further, inhibition of CDK9 activity and consequent reduction in PolII activity has been shown to augment the growth inhibitory effects of CDK1 and CDK2 inhibition in cancer cell lines;[9] here, **4k** inhibited CDK9, as well as CDK7 and reduced PolII phosphorylation at Ser-2 and Ser-5 in vitro and in vivo. Phosphorylation of Rb regulates its interaction with E2F transcription factors, interaction with hypophosphorylated Rb repressing the expression of E2F-regulated genes. Many other interactions have been described, in particular, with proteins containing LXCXE motifs, including histone deacetylases HDAC1 and HDAC2 and chromatin remodelling proteins, with Rb phosphorylation also being critical for these interactions.[32,33] Rb phosphorylation was inhibited at all sites studied, with the observed inhibition being considerably greater for **4k** than that observed for equivalent concentrations of roscovitine, in keeping with the much better growth inhibition seen for **4k** compared with roscovitine. Phosphorylation of all Rb sites was abolished with 10 μmol/L of **4k**, with substantial inhibition being obtained at concentrations as low as 0.1 μmol/L for Thr821, although complete inhibition of Thr821 phosphorylation was not achieved even at high concentrations of **4k**, which may be a reflection of that fact that in addition to being phosphorylated by CDK2, Thr821 can be phosphorylated by CDK6.[34,35] Phosphorylation of PP1a at Thr-320 was inhibited in a dose-dependent manner, likely reflecting the inhibition of CDK1 activity by **4k**. These analyses were reflected in the accumulation of cells in the S and G2/M phases of the cell cycle, with a concomitant reduction in cells in the G1 phase.

As expected from the potent inhibition of CDK1, CDK2, and CDK9 by **4k** and the inhibition of Rb and PolII phosphorylation, the growth of diverse cancer cell lines was inhibited, with GI_{50} values ranging between 0.1 and 1.0 μmol/L. This was confirmed by growth studies performed with the NCI60 cancer cell line panel, GI_{50} values ranging between 0.1 and 0.5 μmol/L, with the exception of the multidrug resistant NCI/Adr-Res ovarian cancer cell line, which was inhibited somewhat less well ($GI_{50} = 2.0$ μmol/L). The growth of human normal vascular endothelial cells was also inhibited less well than the growth of the cancer lines ($GI_{50} = 6.3$ μmol/L), suggestive of some selectivity for cancer cells over normal cells.

The physicochemical and predictive ADME-Tox properties of **4k**, including aqueous solubility, cell permeability, and plasma protein binding were consistent with utility for in vivo studies. Pharmacokinetic studies demonstrated good oral bioavailability, which was confirmed by single oral dose administration, followed by collection of PBMC and FACS

Table 5. Pharmacokinetic Parameters for **4k**[a]

route of admin-istration	dose (mg/kg)	bioavail-ability (%)	T_{max} (min)	C_{max} (min)	$T_{1/2}$ (min)	AUC_{last} (min·ng/mL)	AUCINF (min·mg/mL)	terminal points
PI	10	73	30	15604	147	1583520	158188	3
PO	10	88	15	9347	178	1922912	1926751	3

route of admin-istration	dose (mg/kg)	$T_{1/2}$ (min)	Cl (mL/min/kg)	V_z (mL/kg)	V_{ss} (mL/kg)	AUC_{last} (min·ng/mL)	AUCINF (min·mg/mL)	terminal points
IV	10	210	5	1391	754	2174209	2182968	3

[a] The studies were carried out in mice and the pharmacokinetic parameters were derived from noncompartmental model using WinNonlin 5.2. $T_{1/2}$ = elimination half-life. Cl = total body clearance. V_z = volume of distribution. V_{ss} = an estimate of the volume of distribution at steady state. AUC_{last} = area under the concentration−time curve from the time of dosing to the time of last observation that is greater than the limit of quantitation. AUCINF = area under the concentration−time curve from the time of dosing, extrapolated to infinity. T_{max} = time of maximum observed concentration. C_{max} = concentration corresponding to T_{max}. The bioavailability was calculated based on AUCINF. Terminal points = the number of observations used to calculate the terminal slope.

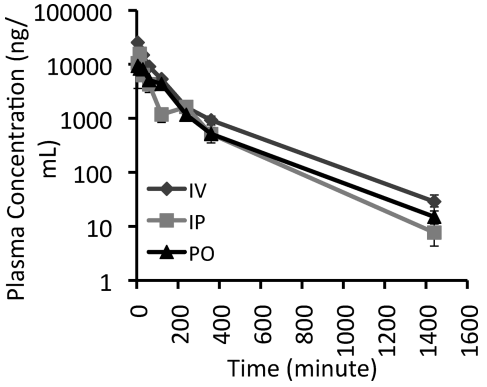

Figure 6. Pharmacokinetic determination of **4k** levels. The mean plasma concentration of **4k** over time was determined for four mice at each time point following **4k** administration. Error bars represent the standard errors of the mean.

analysis of RB and PolII phosphorylation after 6 h. Inhibition of Rb Thr-821 phosphorylation was maximal with a dose of 25 mg/kg. Although PolII Ser-2 phosphorylation was decreased in a dose-dependent manner from 10 to 100 mg/kg, PolII levels were also seen to fall at doses of 50 and 100 mg/kg. Importantly, even at doses of 75 and 100 mg/kg, no significant reduction in PolII or Rb phosphorylation was noted 24 h following **4k** administration, which may be a reflection of the fact that the plasma concentration of **4k** are likely to be below the concentrations that demonstrate inhibition of Rb and PolII phosphorylation in cell lines beyond 6 h post administration. Nevertheless, single daily ip and oral administration of **4k** showed tumor growth inhibition in xenograft models at doses of 10 mg/kg ip in MCF-7 xenografts and 25 mg/kg po in HCT116 xenografts. Further, using Rb phosphorylation as an immunohistochemical marker of CDK activity, we have been able to observe that oral **4k** administration results in reduced Rb phosphorylation in the tumors. This is indicative of a relationship between pharmacodynamic factors and therapeutic outcome for **4k**.

Conclusions

Several selective and broad-specificity CDK inhibitors have now entered clinical trials. Phase I studies show that they can generally be safely administered. Of particular note is PD0332991, a selective CDK4/CDK6 inhibitor, as well as agents with broader selectivity, a few of which have been progressed to phase II studies either as single agents or in combination with chemotherapeutic agents such as cisplatin, gemcitabine, and capecitabine.[23] Here we have described the identification and preclinical evaluation of a potent orally active CDK inhibitor, which demonstrates selectivity for CDK1, CDK2, CDK5, and CDK9, with moderate inhibition in vitro of CDK7 and which is a poor inhibitor of CDK4 and CDK6. Compound **4k** selectively exhibited nanomolar enzymatic potency, potently inhibited all cell lines tested, and demonstrated inhibition of phosphorylation of CDK substrates. A pyrazolopyrimidine compound (Dinaciclib; SCH 727965) which is similar to **4k** in selectively inhibiting CDK1, CDK2, CDK5, and CDK9 with IC_{50} values of 1−4 nmol/L, which shows tumor regression in mouse models[25] and is well tolerated in patients following IV administration in a phase I setting,[23] has recently been described. Our previous description of a CDK7 specific pyrazolopyrimidine-based compound,[24] together with the identification of **4k**, show that pyrazolopyrimidine-based compounds have considerable potential for development as potent CDK inhibitors. Finally, the oral bioavailability of **4k** highlights it as an important new CDK inhibitor, with potential for clinical development.

Materials and Methods

General Synthetic Methods. All manipulations of air or moisture sensitive materials were carried out in oven- or flame-dried glassware under an inert atmosphere of nitrogen or argon. Syringes, which were used to transfer reagents and solvents, were purged with nitrogen prior to use. Reaction solvents were distilled from CaH_2 (CH_2Cl_2, PhMe, Et_3N), Na/Ph_2CO (THF, Et_2O), or obtained as dry or anhydrous from Aldrich Chemical Co. (DMF, MeCN) or BDH (EtOH). Other solvents and all reagents were obtained from commercial suppliers and were used as obtained if purity was >98%. All flash column chromatography was carried out on silica gel 60 particle size 0.040−0.063 mm, unless otherwise stated. Thin layer chromatography (TLC) was performed on precoated aluminum backed or glass backed plates and visualized under ultraviolet light (254 nm) or following spraying with potassium permanganate, vanillin, or phosphomolybdic acid (PMA) stains as deemed appropriate. LC-MS analysis was performed using a Waters LCT Premier XE equipped with a Waters Atlantis C18-reverse phase column of length 30 mm, inner diameter 2.1 mm and particle size 3 μm using a mobile phase of water (0.1% formic acid):acetonitrile, monitoring at 254 nm. Compound purity was determined by combustion analysis (elemental analysis) or LC-MS analysis and was confirmed to be >95% for all compounds.

Dichloride **1** was prepared according to methods described by ref 51.

Benzyl-(5-chloro-3-*iso*-propylpyrazolo[1,5-*a*]pyrimidin-7-yl)-amine. 5,7-Dichloro-3-*iso*-propyl-pyrazolo[1,5-*a*]pyrimidine (**1**) (15.5 g, 67.0 mmol) and benzylamine (14.7 mL, 134 mmol) in EtOH (500 mL) were heated at reflux for 16 h. The reaction mixture was cooled to ambient temperature, concentrated in vacuo, and the residue recrystallized from EtOAc. The mother

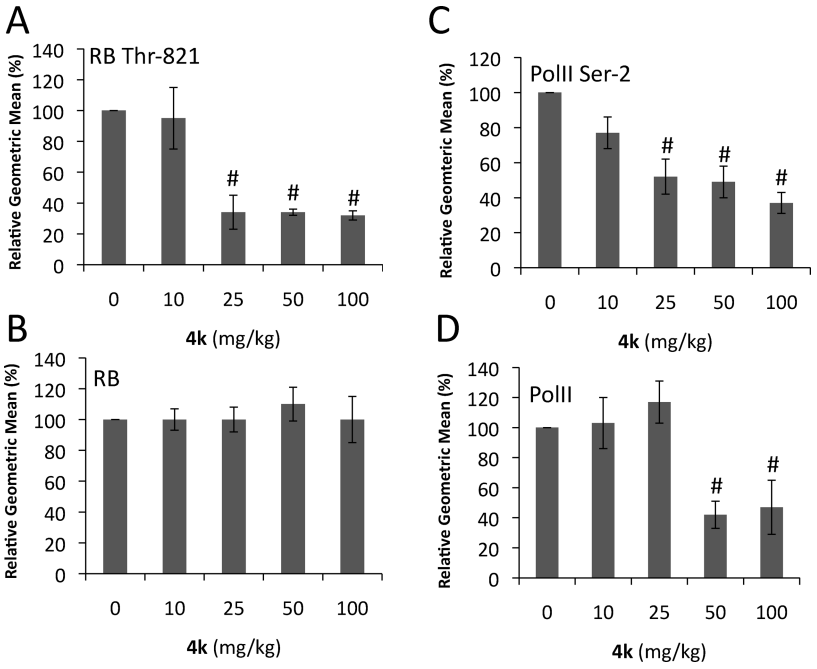

Figure 7. Oral administration of **4k** inhibits cyclin-dependent kinase substrate phosphorylation in mouse peripheral blood mononuclear cells. Mouse PBMCs were collected 6 h following dosing of female nude mice by oral gavage at the dose levels shown. PBMCs were incubated with the appropriate primary antibodies, followed by fluorescently labeled secondary antibodies and flow cytometric analysis ($n = 4$, except for the 100 mg/kg dose where $n = 3$) to determine the status of (A) Rb, (B) Rb phosphorylated at threonine-821 (Rb Thr821), (C) RNA polymerase II Ser-2 phosphorylation (PolII Ser-2), and (D) total PolII. Error bars represent the standard errors of the mean. *P*-Values were determined using Student's *t* test; # represents $p < 0.05$.

liquor was chromatographed on silica (EtOAc:hexanes 1:8) to yield the title pyrazolo[1,5-*a*]pyrimidine as a white solid. The combined yield of the crystallized and chromatographed material was 19.3 g, 96%; mp 78−79 °C (EtOAc); TLC Rf 0.16 (EtOAc:hexanes 1:16). IR (neat) 3380, 3239, 1616, 1585 cm^{-1}. ^1H NMR ($CDCl_3$, 400 MHz) δ 7.84 (s, 1H), 7.40−7.32 (m, 5H), 6.88 (m, 1H), 5.91 (s, 1H), 4.55 (m, 2H), 3.28 (sept, $J = 6.9$ Hz, 1H), 1.33 (d, $J = 6.9$ Hz, 6H). ^{13}C NMR ($CDCl_3$, 100 MHz) δ 150.2, 146.9, 144.2, 141.6, 135.8, 129.1, 128.3, 127.3, 117.0, 84.7, 46.2, 23.5, 23.4. MS *m*/*z* (ESI) 301 $(M + H)^+$. HRMS (ESI) calcd for $C_{16}H_{18}ClN_4^+$, 301.1215; found, 301.1227. Anal. Calcd for $C_{16}H_{17}ClN_4$: C, 63.89; H, 5.70; N, 18.63. Found: C, 63.95; H, 5.78; N, 18.59.

***tert*-Butyl-benzyl-(5-chloro-3-*iso*-propylpyrazolo[1,5-*a*]pyrimidin-7-yl)-carbamate Monohydrate (2).** Benzyl-(5-chloro-3-*iso*-propyl-pyrazolo[1,5-*a*]pyrimidin-7-yl)-amine (17.0 g, 56.7 mmol), Boc_2O (16.1 g, 73.7 mmol), and DMAP (100 mg) in THF (400 mL) were stirred for 20 h at ambient temperature. EtOAc (300 mL) was added, and the organic layer was washed with water (2 × 400 mL) and saturated aqueous $NaHCO_3$ (400 mL) and dried (Na_2SO_4). Concentration in vacuo, chromatography (EtOAc:hexanes 1:8), and recrystallization from EtOAc and hexanes (1: 8) gave carbamate **2** (22.6 g, 100%) as a pale-yellow solid; mp 100−103 °C (EtOAc); TLC Rf 0.40 (EtOAc:hexanes 1:8). IR (neat) 1612 cm^{-1}. ^1H NMR ($CDCl_3$, 400 MHz) δ 8.02 (s, 1H), 7.34−7.21 (m, 5H), 6.48 (s, 1H), 5.03 (s, 2H), 3.31 (sept, $J = 6.9$ Hz, 1H), 1.52 (s, 2H), 1.39 (s, 9H), 1.37 (d, $J = 6.9$ Hz, 6H). ^{13}C NMR ($CDCl_3$, 100 MHz) δ 152.8, 148.0, 145.1, 144.3, 142.6, 136.8, 128.7, 127.8, 127.8, 118.3, 106.3, 83.0, 51.4, 28.0, 23.6, 23.4. MS *m*/*z* (ESI) 401 $(M + H)^+$. HRMS (ESI) calcd for $C_{21}H_{26}ClN_4O_2^+$, 401.1739; found, 401.1735. Anal. Calcd for $C_{21}H_{27}ClN_4O_3$: C, 60.21; H, 6.50; N, 13.37. Found: C, 60.28; H, 6.58; N, 13.43.

General Procedure for Buchwald−Hartwig Coupling Reaction. *tert*-Butyl-benzyl-(5-chloro-3-*iso*-propylpyrazolo[1,5-*a*]pyrimidin-7-yl)-carbamate (1.0 equiv), tris(dibenzylideneacetone)dipalladium (0.05 equiv), 2,2′-bis(diphenylphosphino)-1,1′-binaphthalene (0.15 equiv), and sodium *tert*-butoxide (1.1 equiv) were suspended in PhMe (0.30 M) and stirred for 15 min. The amine (1.1 equiv) was added and the mixture heated to 95 °C for 16 h and cooled and diluted with EtOAc. The organic phase was washed with water (3×), brine, dried ($MgSO_4$), and concentrated in vacuo. Chromatography on silica (EtOAc:hexanes) gave the pure coupled products.

General Procedure for the Final Acid Deprotection. AcCl was dissolved in MeOH (5.0 M) with stirring at 0 °C. After 15 min, the solution was warmed to room temperature and stirred for a further 15 min. The ambient was added and the mixture stirred at ambient temperature for 3 h and concentrated in vacuo. The residue was dissolved in CH_2Cl_2, washed with saturated aqueous sodium bicarbonate, dried (Na_2SO_4), and concentrated in vacuo. Crystallization (MeCN or MeOH) or chromatography (CH_2Cl_2: MeOH) gave the pure analogues.

Compound **5** was prepared according to Campbell et al.[36]

(*R*)-1-(*tert*-Butyldimethylsilyloxy)-3-buten-2-amine (6). Et_3N (5.00 mL, 35.6 mmol), DMAP (20.0 mg), and t-$BuMe_2SiCl$ (2.70 g, 17.8 mmol) were added to amino-alcohol **5** (2.00 g, 16.2 mmol) in CH_2Cl_2 (80 mL). The mixture was stirred overnight at ambient temperature. Water (80 mL) was added, and the mixture was vigorously stirred for 10 min. The organic phase was separated, washed with water (60 mL) and brine (60 mL), and dried (Na_2SO_4). Concentration in vacuo gave amine **6** (2.83 g, 43%) as a yellow oil; TLC Rf 0.55 (EtOAc:hexanes 1:1); $[\alpha]^{25}_D$ (*c* 1.09, CH_2Cl_2) + 22.8. IR (neat) 1471, 1254, 1095 cm^{-1}. ^1H NMR ($CDCl_3$, 300 MHz) δ 5.80 (m, 1H), 5.14 (m, 2H), 3.60 (m, 1H), 3.42 (m, 2H), 1.61 (m, 2H), 0.89 (s, 9H), 0.05 (s, 6H). ^{13}C NMR ($CDCl_3$, 75 MHz) δ 139.2, 115.1, 67.8, 55.8, 25.9, 18.3, −5.4. MS *m*/*z* (CI) 202 $(M + H)^+$. HRMS (CI) calcd for $C_{10}H_{24}NOSi^+$, 202.1622; found, 202.1622.

(*R*)-*tert*-Butyl Benzyl(5-((1-((*tert*-butyldimethylsilyl)oxy)but-3-en-2-yl)amino)-3-*iso*-propylpyrazolo[1,5-*a*]pyrimidin-7-yl)carbamate (3f). Synthesized according to the general procedure for Buchwald−Hartwig coupling, **2** (100 mg, 0.25 mmol), Pd_2dba_3 (12.0 mg, 0.013 mmol), BINAP (24.0 mg, 0.039 mmol), sodium *tert*-butoxide (36.0 mg, 0.38 mmol), amine **6** (58.0 mg, 0.27 mmol), and PhMe (0.80 mL) yielded carbamate **3f** (72.0 mg,

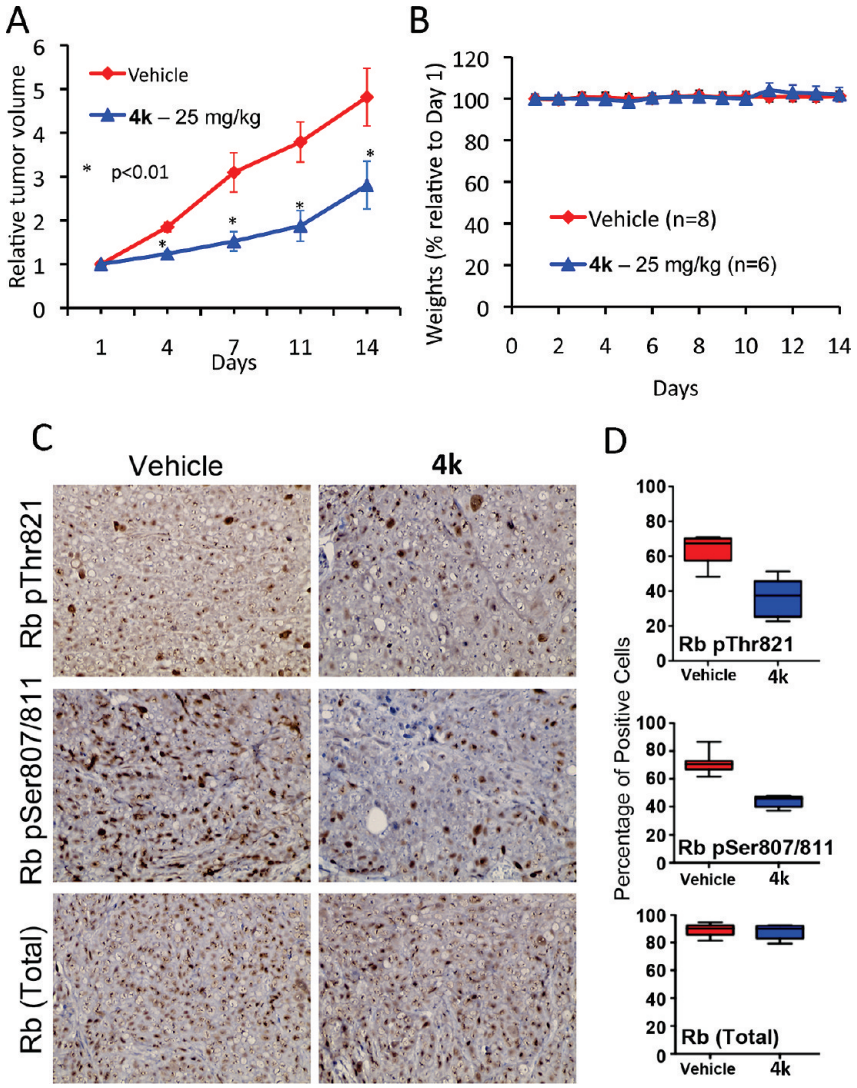

Figure 8. Oral administration of **4k** inhibits human tumor xenografts. (A) Female nude mice bearing HCT116 tumor xenografts were dosed by oral gavage with vehicle ($n = 8$) or **4k** at a concentration of 25 mg/kg ($n = 6$). (B) The weights of the animals used over the time course of the study are shown. Error bars represent the standard errors of the mean. *P*-Values were determined using Student's *t* test; # represents $p < 0.05$, * represents $p < 0.01$, and ** represents $p < 0.001$. (C) Shown are representative images for tumor xenografts immunostained using antibodies for Rb, Rb pSer807/811, and Rb pThr821. (D) One thousand nuclei were scored for determining percentage of stained cells in sections from each tumor. The results of the scoring are shown as box plots. Student's *t* test analysis showed that pSer807/811 and pThr821 staining was significantly different ($p < 0.005$) between the vehicle and **4k** treatment groups, whereas there was no significant difference in levels of total Rb.

0.13 mmol, 51%). Purification EtOAc:hexanes (1:10): $[\alpha]_D$ (c 0.59, CH_2Cl_2) + 16.3. IR (neat) 3370, 1722, 1642, 1581, 1516, 1368, 1158, 1107, 837, 777, 699 cm^{-1}. ^1H NMR ($CDCl_3$, 300 MHz) δ 7.75 (s, 1H), 7.27 (m, 5H), 5.85 (m, 1H), 5.71 (s, 1H), 5.19 (m, 2H), 4.97 (br s, 1H), 4.95 (br s, 2H), 4.54 (m, 1H), 3.75 (m, 2H), 3.08 (m, 1H), 1.40−1.31 (m, 15H), 0.88 (s, 9H), 0.05 (s, 6H). ^{13}C NMR ($CDCl_3$, 75 MHz) δ 154.0, 153.5, 146.1, 142.8, 141.5, 137.7, 136.4, 128.4, 127.9, 127.4, 116.2, 113.3, 97.2, 82.0, 65.0, 54.6, 51.3, 28.0, 25.9, 23.8, 23.1, 18.3, −5.4. MS *m*/*z* (CI) 566 $(M + H)^+$. HRMS (CI) calcd for $C_{31}H_{48}N_5O_3Si^+$, 566.3526; found, 566.3538.

***tert*-Butyl Benzyl(5-(((2*S*,3*S*)-1-((*tert*-butyldimethylsilyl)oxy)-3,4-dihydroxybutan-2-yl)amino)-3-*iso*-propylpyrazolo[1,5-*a*]pyrimidin-7-yl)carbamate (3k). *tert*-Butyl Benzyl(5-(((2*S*,3*R*)-1-((*tert*-butyldimethylsilyl)oxy)-3,4-dihydroxybutan-2-yl)amino)-3-*iso*-propylpyrazolo[1,5-*a*]pyrimidin-7-yl)carbamate (3l).** OsO_4 (5.40 mL, 15 mol %, 2.5 wt % in ^{t}BuOH) was added to alkene **3f** (2.27 g, 4.00 mmol) and NMO H_2O (0.97 g, 8.3 mmol) in MeCN and H_2O (4:1, 80 mL). After 16 h, reaction was quenched by the addition of saturated aqueous Na_2SO_3 (20 mL). The mixture was stirred for 45 min at ambient temperature, and the aqueous phase was extracted with EtOAc (3 × 200 mL). The combined organic phases were dried (Na_2SO_4), concentrated in vacuo, and chromatographed (EtOAc:hexanes 1:20) to yield carbamate **3k** (1.00 g, 1.67 mmol, 42%) and carbamate **3l** (800 mg, 1.34 mmol, 33%). **3k**: IR (neat) 3363, 1721, 1644, 1518 cm^{-1}. ^1H NMR ($CDCl_3$, 400 MHz) δ 7.80 (s, 1H), 7.36−7.27 (m, 5H), 5.72 (s, 1H), 5.24−5.22 (m, 1H), 4.98−4.94 (m, 3H), 4.18−4.11 (m, 1H), 3.95−3.90 (m, 1H), 3.79−3.76 (m, 1H), 3.64−3.57 (m, 3H), 3.10 (hept, $J = 6.9$ Hz, 1H), 2.84−2.81 (m, 1H), 1.43 (s, 9H), 1.33 (d, $J = 6.9$ Hz, 6H), 0.93 (s, 9H), 0.13−0.12 (m, 6H). ^{13}C NMR ($CDCl_3$, 100 MHz) δ 154.8, 153.4, 141.7, 137.6, 128.5, 127.9, 127.6, 113.8, 97.4, 83.8, 82.5, 70.4, 62.5, 61.8, 53.5, 51.7, 28.0, 25.9, 23.6, 23.5, 23.2, −5.4. MS *m*/*z* (CI) 600 $(M + H)^+$. HRMS (CI) calcd for $C_{31}H_{50}N_5O_5Si^+$, 600.3576; found, 600.3578.

3l: IR (neat) 3361, 1719, 1644, 1518 cm^{-1}. ^1H NMR ($CDCl_3$, 400 MHz) δ 7.77 (s, 1H), 7.32−7.23 (m, 5H), 5.78 (s, 1H), 5.27−5.25 (m, 1H), 4.98−4.89 (m, 2H), 4.41 − 4.31 (m, 2H), 4.14−4.09 (m, 1H), 4.00−3.90 (m, 2H), 3.79−3.75 (m, 1H), 3.61−3.57 (m, 1H), 3.40−3.36 (m, 1H), 3.11−3.04 (m, 1H), 1.40

(s, 9H), 1.32−1.28 (m, 6H), 0.89 (s, 9H), 0.08−0.06 (m, 6H). ^{13}C NMR ($CDCl_3$, 100 MHz) δ 141.7, 137.6, 128.5, 127.9, 127.6, 113.8, 97.4, 82.5, 70.4, 62.4, 61.8, 60.4, 53.5, 51.6, 28.0, 25.9, 23.6, −5.4. MS *m*/*z* (CI) 600 $(M + H)^+$. HRMS (CI) calcd for $C_{31}H_{50}N_5O_5Si^+$, 600.3576; found, 600.3574.

(2*S*,3*S*)-3-(7-(Benzylamino)-3-iso-propylpyrazolo[1,5-*a*]pyrimidin-5-ylamino)-1,2,4-butanetriol (4k). Synthesized according to the general procedure for acidic deprotection. **3k** (605 mg, 1.01 mmol), HCl/MeOH (50.0 mL). Yield triol **4k** (310 mg, 0.81 mmol, 79%). Purification crystallization from MeCN: mp 184−186 °C; $[\alpha]^{25}_D$ (*c* 0.20, CH_3OH) −25.0. IR (neat) 3229, 1639, 1581 cm^{-1}. ^{1}H NMR (CD_3OD, 400 MHz) δ 7.69 (s, 1H), 7.42−7.27 (m, 5H), 5.32 (s, 1H), 4.56 (s, 2H), 4.10−4.04 (m, 1H), 3.87 (dd, *J* = 11.4, 4.1 Hz, 1H), 3.84 (dd, *J* = 11.1, 5.5 Hz), 3.63−3.56 (m, 3H), 3.05 (hept, *J* = 6.9 Hz, 1H), 1.31 (d, *J* = 6.9 Hz, 3H), 1.29 (d, *J* = 6.9 Hz, 3H). ^{13}C NMR (CD_3OD, 100 MHz) δ 157.6, 146.9, 144.9, 140.6, 137.7, 128.4, 127.1, 126.6, 112.1, 72.8, 72.0, 63.0, 61.7, 54.3, 45.1, 23.3, 22.6, 22.2. MS *m*/*z* (ESI) 386 $(M + H)^+$. HRMS (ESI) calcd for $C_{20}H_{28}N_5O_3^+$, 386.2187; found, 386.2181.

(2*R*,3*S*)-3-(7-(Benzylamino)-3-iso-propylpyrazolo[1,5-*a*]pyrimidin-5-ylamino)-1,2,4-butanetriol (4l). Synthesized according to the general procedure for acidic deprotection. **3l** (765 mg, 1.28 mmol), HCl/MeOH (50.0 mL). Yield **4l** (338 mg, 0.86 mmol, 67%). Purification chromatography (EtOAc): $[\alpha]^{25}_D$ (*c* 0.20, CH_3OH) −60.0. IR (neat) 3307, 1637, 1579 cm^{-1}. ^{1}H NMR (CD_3OD, 400 MHz) δ 7.68 (s, 1H), 7.40−7.25 (m, 5H), 5.34 (s, 1H), 4.54 (s, 2H), 4.23−4.20 (m, 1H), 3.93−3.89 (ddd, *J* = 8.3, 5.9, 2.2 Hz, 1H), 3.80 (dd, *J* = 11.0, 6.2 Hz, 1H), 3.77 (dd, *J* = 11.0, 7.0 Hz, 1H), 3.52 (dd, *J* = 11.5, 6.1 Hz, 1H), 3.39 (dd, *J* = 11.0, 8.7 Hz, 1H), 3.03 (hept, *J* = 6.9 Hz, 1H), 1.31 (d, *J* = 6.9 Hz, 3H), 1.29 (d, *J* = 6.9 Hz, 3H). ^{13}C NMR (CD_3OD, 100 MHz) δ158.0, 146.9, 144.5, 140.1, 137.7, 128.3, 127.1, 126.7, 112.0, 72.8, 70.8, 62.2, 62.0, 53.4, 45.1, 23.2, 22.6, 22.2. MS *m*/*z* (ESI) 386 $(M + H)^+$. HRMS (ESI) calcd for $C_{20}H_{28}N_5O_3^+$, 386.2187; found, 386.2189.

Second Generation Synthesis of 4k. (2*R*,3*S*)-Diethyl 2-azido-3-hydroxysuccinate (9). (−)-Diethyl tartrate (10.0 g, 48.5 mmol) in CH_2Cl_2 (250 mL) was cooled to −5 °C. Et_3N (13.5 mL, 97.0 mmol) was added, followed by the dropwise addition of $SOCl_2$ (5.28 mL, 72.7 mmol). After 30 min, the mixture was poured into water and the aqueous layer extracted into CH_2Cl_2 (3×). The combined organic layers were washed with brine, dried (Na_2SO_4), and concentrated in vacuo to yield the cyclic sulfite which was directly dissolved in DMF (400 mL), and sodium azide (6.30 g, 97.0 mmol) was added. The mixture was stirred for 12 h and then poured into water and extracted into Et_2O (3×). The combined organic layers were washed with brine, dried ($MgSO_4$), and concentrated in vacuo. Chromatography (hexanes:EtOAc 4:1) gave azide **9** (7.79 g, 33.7 mmol, 70%): $[\alpha]_D$ (c 1.0, EtOH) −39.4. ^{1}H NMR ($CDCl_3$, 400 MHz) δ 4.66 (dd, *J* = 5.5, 2.7 Hz, 1H), 4.32 (m, 4H), 3.31 (d, *J* = 5.5 Hz, 1H), 1.35 (t, *J* = 7.1 Hz, 3H), 1.34 (t, *J* 7.1 Hz, 3H). ^{13}C NMR ($CDCl_3$, 100 MHz) δ 170.6, 166.9, 71.5, 64.2, 62.6, 62.0, 14.0.

(*S*)-4-((*S*)-1-Azido-2-(methoxymethoxy)ethyl)-2,2-dimethyl-1,3-dioxolane (11). Diester **9** (5.00 g, 21.6 mmol) in EtOH (80.0 mL) was cooled to −10 °C and lithium chloride (909 mg, 21.6 mmol) was added, followed by portionwise addition of sodium borohydride (4.80 g, 130 mmol). The suspension was warmed overnight, recooled to −10 °C, and acidified to pH4 by the dropwise addition of 1 M HCl in H_2O. The resultant clear solution was concentrated in vacuo to yield crude triol **10**, which was directly suspended in Me_2CO (80.0 mL) and 2,2-dimethoxypropane (25.0 mL). *p*-TsOH.H_2O (400 mg, 2.1 mmol) was added and the mixture heated to 50 °C for 2.5 h, cooled, and saturated ammonium chloride solution (60.0 mL) was added. The suspension was stirred for 1 h, poured into water, and extracted into Et_2O (3×). The combined organic layers were washed with brine, dried ($MgSO_4$), and concentrated in vacuo. The residue was dissolved in CH_2Cl_2 (25.0 mL), cooled to 0 °C, and *N*,*N*-di-*iso*-propylethylamine (7.51 mL, 43.2 mmol) was added followed by the slow addition of $MeOCH_2Cl$ (3.26 mL, 43.2 mmol) and the mixture was stirred overnight. The solution was poured into water and extracted into CH_2Cl_2 (3×). The combined organic layers were washed with brine, dried (Na_2SO_4), and concentrated in vacuo. Chromatography (hexanes:EtOAc 10:1) gave azide **11** (3.49 g, 15.1 mmol, 70%); $[\alpha]^{25}_D$ (*c* 1.2, $CHCl_3$) + 18.6. IR (neat) 3229, 2100, 1373, 1259 cm^{-1}. ^{1}H NMR ($CDCl_3$, 400 MHz) δ 4.68 (s, 2H), 4.14−4.06 (m, 2H), 3.97−3.94 (m, 1H), 3.84−3.78 (m, 1H), 3.71−3.64 (m, 2H), 3.42 (s, 3H), 1.47 (s, 3H), 1.37 (s, 3H). ^{13}C NMR ($CDCl_3$, 100 MHz) δ 109.8, 96.7, 74.8, 67.3, 66.6, 63.0, 55.5, 26.5, 25.2. MS *m*/*z* (ESI) 249 $(M + NH_4)^+$. HRMS (ESI) calcd for $C_9H_{18}N_3O_4^+$, 232.1297; found, 232.1303.

(*S*)-1-((*S*)-2,2-Dimethyl-1,3-dioxolan-4-yl)-2-(methoxymethoxy)-ethanamine (12). Azide **11** (3.49 g, 15.1 mmol) in MeOH (100 mL) and added to Pd/C (10 wt %, 350 mg). The atmosphere was replaced by hydrogen and hydrogen bubbled through the suspension for 1 h. The mixture was filtered through Celite and concentrated in vacuo to yield amine **12** (3.02 g, 14.7 mmol, 97%). IR (neat) 3330, 1600, 1461 cm^{-1}. ^{1}H NMR ($CDCl_3$, 400 MHz) δ 4.65 (s, 2H), 4.07−4.01 (m, 2H), 3.93−3.87 (m, 1H), 3.66 (dd, *J* = 9.7, 3.5 Hz, 1H), 3.51 (dd, *J* = 9.7, 6.2 Hz, 1H), 3.38 (s, 3H), 3.10−3.06 (m, 1H), 1.45 (br. s, 2H), 1.43 (s, 3H), 1.36 (s, 3H). ^{13}C NMR ($CDCl_3$, 100 MHz) δ 108.9, 96.7, 77.1, 69.8, 66.3, 55.3, 53.2, 26.6, 25.3. HRMS (ESI) calcd for $C_9H_{20}NO_4$, 206.1392; found, 206.1395.

(2*S*,3*S*)-3-(7-(Benzylamino)-3-*iso*-propylpyrazolo[1,5-*a*]pyrimidin-5-ylamino)-1,2,4-butanetriol (4k). Synthesized according to the general procedure for Buchwald−Hartwig coupling, **2** (500 mg, 1.25 mmol), Pd_2dba_3 (57.0 mg, 0.062 mmol), BINAP (117.0 mg, 0.19 mmol), sodium *tert*-butoxide (132 mg, 1.38 mmol), **12** (283 mg, 1.38 mmol), and PhMe (5.0 mL). Purification EtOAc:hexanes (1:4). Analytically pure material could not be obtained at this stage. General procedure for acidic deprotection followed. HCl/MeOH (50.0 mL) yield **4k** (412 mg, 1.07 mmol, 86%). Purification: crystallization from MeCN.

Expression, Purification, and Crystallography of CDK2 Complexed with 4k. A cDNA encoding human CDK2[37] was cloned into a pProEx-HTb vector (Invitrogen) containing a 6×His-SUMO-1 N-terminal tag and expressed in *E. coli* BL21 (DE3). To cleave the SUMO tag, SuPr-1/Senp2 (Imagenes, Berlin, Germany) was cloned into pET28b (Novagen) with both N- and C-terminal 6×His tags and expressed in *E. coli* BL21(DE3). After a first nickel affinity purification, 6×His-SUMO-CDK2 was incubated with partially purified SUMO protease at 4 °C overnight. Cleaved CDK2 was separated from the 6×His-SUMO tag and the SUMO protease using a second nickel affinity column and further purified on a Superdex 75 gel filtration column (GE Healthcare). This purification method takes advantage of the fact that the SUMO protease cleaves the SUMO tag without leaving any extra N-terminal residues, which would hinder crystallization. Purified CDK2 was stored at −80 °C in the crystallization buffer (10 mM Hepes pH 7.4, 0.5 mM DTT). Crystallization and ligand soaking conditions were as previously described.[38] A 1.8 Å diffraction data set was collected at beamline I02 (Diamond Light Source, Didcot, England) and the structure solved by molecular replacement with Molrep4,[39] using the 1HCK PDB structure as the search model. **4k** was fitted automatically using ARP/wARP ligand[40] and the structure refined using Refmac5.[41] Coordinates and structure factors have been deposited to the Protein Data Bank, PDB code 3NS9.

In Vitro Kinase Assays. Purified recombinant CDK1/cycB1, CDK2/cycE, CDK4/cycD1, CDK5/p35NCK, CDK6/CycD1, CDK7/CycH/MAT1, and CDK9/CycT were purchased from Proqinase GmbH (Freiburg, Germany). Kinase assays were performed according to manufacturer's protocols, using substrate peptides purchased from Proqinase GmbH. Measurement of the amount of ATP remaining at the end of the reaction, carried out with a luciferase assay (PKLight assay; Cambrex, England), was used to determine inhibition of kinase activity by compounds.

Cell Growth Assays. Cell lines were obtained from the CRUK cell bank facility and were routinely cultured in DMEM supplemented with 10% fetal calf serum (FCS) (First Link, England). Cell growth was assessed using the Sulforhodamine B (SRB) assay, as described.[42] Human normal umbilical vein endothelial cells (HUVEC) and the appropriate culture media were purchased from Lonza Wokingham Ltd., England, and the cells were cultured as per supplier's protocols.

Flow Cytometry. HCT116 colon cancer cells were seeded (4×10^5) in 6-well plates in DMEM containing 10% FCS and allowed to adhere for 24 h. Compounds prepared in DMSO were added, and after 24 h incubation, cells were trypsinized, centrifuged at 1100 rpm for 5 min, and resuspended in 5 mL of ice-cold PBS, centrifuged as above, gently resuspended in 2 mL ice-cold 70% ethanol, and incubated at 4 °C for 1 h. Cells were washed twice with 5 mL of ice-cold PBS and resuspended in 100 μL of PBS containing 100 μg/mL RNase (Sigma-Aldrich, England) and 1 mL of 50 μg/mL propidium iodide (Sigma-Aldrich, England) in PBS. Following incubation overnight in the dark at 4 °C and filtering through 70 μm muslin gauze into FACS tubes (Becton-Dickinson, England) to remove cell clumps, stained cells were processed using the RXP cytomics software on a Beckman Coulter Elite ESP (Beckman Coulter, High Wycombe, United Kingdom). The data were analyzed using Flow Jo v7.2.5 (Tree Star Inc., San Calos, CA), and statistical analysis was performed using the unpaired Student's *t* test to determine *p*-values.

Immunoblotting. Cells (8×10^5), plated in 10 cm plates, were treated with compounds after 24 h. Four hours later, cell lysates were prepared by the addition of 500 μL of RIPA buffer (Sigma-Aldrich, England), containing phosphatase inhibitor cocktail and complete protease inhibitor cocktail, both from Roche Diagnostics, England. Protein concentrations were determined using the BCA protein assay (Thermo-Scientific, England). Immunoblotting was performed as described previously.[43] Antibody details are available upon request.

In Vivo Assessment of Molecular Pharmcology. All procedures were approved by the Imperial College London Animal Ethics Committee. The experiments were done by licensed investigators in accordance with the United Kingdom Home Office's regulations under the Animal (Scientific Procedures) Act 1986 and were within guidelines set out by the United Kingdom Coordinating Committee for Cancer Research's Ad hoc Committee on the Welfare of Animals in Experimental Neoplasia.[44] Seven-week-old female nu/nu-BALB/c athymic nude mice were purchased from Harlan Olac Ltd. (England). **4k**, prepared in 28% (w/v) PEG300/5% (v/v) dimethylacetamide/10% (w/v) HPB cyclodextrin in H_2O, was administered by oral gavage. Drug was administered by exact body weight, with the injection volume being not more than 0.2 mL. After 6 h, the mice were anaesthetized and blood collected by cardiac puncture into tubes containing 200 μL of PBS, 100 U of Heparin, and 10 mM EDTA. Blood was mixed with 1 mL of red blood cell lysis solution (Flowgen Bioscience, Nottingham, England) for 15 min at room temperature, followed by centrifugation for 5 min at 1,000 rpm to pellet the peripheral blood mononuclear cells (PBMC). PMBC were washed twice in PBS, and the cells were stained using the Fix and Perm kit (Caltag Laboratories, Burlingame, CA, USA) following the manufacturer's instructions. Briefly, after washing the PBMCs in PBS, $2 \times 10^4 - 10^5$ cells were fixed using 50 μL of reagent A (fixation medium) for 15 min at room temperature. At the end of the incubation, the cells were washed in PBS, and then 50 μL of reagent B (permeabilization medium) was added together with antibodies for RNA polymerase II (PolII), PolII P-Ser2, RB, or RB P-Thr821 (purchased from Abcam, England) at a dilution of 1:100 for 1 h at room temperature. Cells were washed three times with PBS and were incubated for 1 h with goat antirabbit Alexafluor 488 (Invitrogen, Paisley, England) diluted at 1:200 in PBS in the dark at room temperature. Finally cells were washed in PBS three times and resuspended in 200 μL of PBS and stored at 4 °C for flow cytometric analysis. Labeled cells were processed using the RXP cytomics software on a Beckman Coulter Elite ESP, and the data were analyzed using Flow Jo v7.2.5.

Absorption, Distribution, Metabolism, Elimination and Toxicity (ADME-Tox) and Pharmacokinetic Studies. Studies were performed under contract by Cerep Inc. (USA), using described methods.[45−48]

Tumor Xenografts. HCT116 cells (5×10^6) were injected subcutaneously in not more than 0.1 mL volume into the flank of the animals (female nu/nu-BALB/c athymic nude mice). Tumor measurements were performed twice per week, and volumes were calculated using the formula $^1/_2$[length (mm)] × [width (mm)]^2. The animals were randomized, and when tumors had reached a volume of 100−200 mm^3, animals were entered into the different treatment groups and treatment with **4k** or vehicle control was initiated. Animals were treated with **4k** prepared as abovedaily by oral gavage for a total of 14 days. At the end of the 14-day treatment period, the mice were sacrificed, and the tumors were fixed by formalin fixation and paraffin embedding. Throughout the 14-day treatment period, animal weights were determined each day and tumor volumes on alternate days. The MCF-7 xenograft study was performed exactly as described previously.[24]

Immunohistochemistry. Tumors were dissected from mice and fixed in 10% formalin and embedded in paraffin blocks. Immunohistochemical staining was performed as described previously,[49] except that antigen retrieval was performed by microwaving for 10 min using 10 mmol/L citrate buffer (pH 6.0). Antibodies used were Rb pThr821 (ab4787) from Abcam (England) or Rb (9309) and Rb pSer807/811 (9308) from New England Biolabs, England. Images were acquired using the Automated Cellular Imaging System (ACIS) (Carl Zeiss Ltd., Welwyn Garden City, England). Cell positivity was determined by counting >1000 cells per section, and the results were tabulated using GraphPad Prism software, with statistical significance being determined using the Student's *t* test (GraphPad Prism).

Acknowledgment. This work was funded by grants from the Engineering and Physical Sciences Research Council and Cancer Research UK. Our thanks go to the MRC Protein Phosphorylation unit for the 76-kinase screening and to Cerep, Inc. for the ADME-Tox and PK studies. The Developmental Therapeutics Program at NCI carried out the NCI60 screening of **4k**. We are grateful for support from the NIHR Biomedical Research Centre funding scheme. We also thank the CR-UK and the Dept of Health funded Imperial College Experimental Cancer Medicine Centre (ECMC) grant.

Supporting Information Available: In vitro kinase and cell growth inhibition data, cell cycle profiles, and spectral data for **4k**, as well as additional synthetic methods. This material is available free of charge via the Internet at http://pubs.acs.org.

References

(1) Sherr, C. J. Cancer cell cycles. *Science* **1996**, *274*, 1672–1677.
(2) Morgan, D. O. Cyclin-dependent kinases: engines, clocks, and microprocessors. *Annu. Rev. Cell Dev. Biol.* **1997**, *13*, 261–291.
(3) Malumbres, M.; Barbacid, M. Cell cycle, CDKs and cancer: a changing paradigm. *Nature Rev. Cancer* **2009**, *9*, 153–166.
(4) Fu, M.; Wang, C.; Li, Z.; Sakamaki, T.; Pestell, R. G. Minireview: Cyclin D1: normal and abnormal functions. *Endocrinology* **2004**, *145*, 5439–5447.
(5) Malumbres, M.; Barbacid, M. To cycle or not to cycle: a critical decision in cancer. *Nature Rev. Cancer* **2001**, *1*, 222–231.
(6) Ortega, S.; Prieto, I.; Odajima, J.; Martin, A.; Dubus, P.; Sotillo, R.; Barbero, J. L.; Malumbres, M.; Barbacid, M. Cyclin-dependent kinase 2 is essential for meiosis but not for mitotic cell division in mice. *Nature Genet.* **2003**, *35*, 25–31.

(7) Berthet, C.; Aleem, E.; Coppola, V.; Tessarollo, L.; Kaldis, P. Cdk2 knockout mice are viable. *Curr. Biol.* **2003**, *13*, 1775–1785.
(8) Aleem, E.; Kiyokawa, H.; Kaldis, P. Cdc2-cyclin E complexes regulate the G1/S phase transition. *Nature Cell Biol.* **2005**, *7*, 831–836.
(9) Cai, D.; Latham, V. M., Jr.; Zhang, X.; Shapiro, G. I. Combined depletion of cell cycle and transcriptional cyclin-dependent kinase activities induces apoptosis in cancer cells. *Cancer Res.* **2006**, *66*, 9270–9280.
(10) Rane, S. G.; Dubus, P.; Mettus, R. V.; Galbreath, E. J.; Boden, G.; Reddy, E. P.; Barbacid, M. Loss of Cdk4 expression causes insulin-deficient diabetes and Cdk4 activation results in beta-islet cell hyperplasia. *Nature Genet.* **1999**, *22*, 44–52.
(11) Tsutsui, T.; Hesabi, B.; Moons, D. S.; Pandolfi, P. P.; Hansel, K. S.; Koff, A.; Kiyokawa, H. Targeted disruption of CDK4 delays cell cycle entry with enhanced p27(Kip1) activity. *Mol. Cell. Biol.* **1999**, *19*, 7011–7019.
(12) Malumbres, M.; Sotillo, R.; Santamaria, D.; Galan, J.; Cerezo, A.; Ortega, S.; Dubus, P.; Barbacid, M. Mammalian cells cycle without the D-type cyclin-dependent kinases Cdk4 and Cdk6. *Cell* **2004**, *118*, 493–504.
(13) Yu, Q.; Sicinska, E.; Geng, Y.; Ahnstrom, M.; Zagozdzon, A.; Kong, Y.; Gardner, H.; Kiyokawa, H.; Harris, L. N.; Stal, O.; Sicinski, P. Requirement for CDK4 kinase function in breast cancer. *Cancer Cell* **2006**, *9*, 23–32.
(14) Landis, M. W.; Pawlyk, B. S.; Li, T.; Sicinski, P.; Hinds, P. W. Cyclin D1-dependent kinase activity in murine development and mammary tumorigenesis. *Cancer Cell* **2006**, *9*, 13–22.
(15) Reddy, H. K.; Mettus, R. V.; Rane, S. G.; Grana, X.; Litvin, J.; Reddy, E. P. Cyclin-dependent kinase 4 expression is essential for neu-induced breast tumorigenesis. *Cancer Res.* **2005**, *65*, 10174–10178.
(16) Yu, Q.; Geng, Y.; Sicinski, P. Specific protection against breast cancers by cyclin D1 ablation. *Nature* **2001**, *411*, 1017–1021.
(17) Malumbres, M.; Barbacid, M. Is Cyclin D1-CDK4 kinase a bona fide cancer target? *Cancer Cell* **2006**, *9*, 2–4.
(18) Roy, R.; Adamczewski, J. P.; Seroz, T.; Vermeulen, W.; Tassan, J. P.; Schaeffer, L.; Nigg, E. A.; Hoeijmakers, J. H.; Egly, J. M. The MO15 cell cycle kinase is associated with the TFIIH transcription-DNA repair factor. *Cell* **1994**, *79*, 1093–1101.
(19) Serizawa, H.; Makela, T. P.; Conaway, J. W.; Conaway, R. C.; Weinberg, R. A.; Young, R. A. Association of Cdk-activating kinase subunits with transcription factor TFIIH. *Nature* **1995**, *374*, 280–282.
(20) Fisher, R. P. Secrets of a double agent: CDK7 in cell-cycle control and transcription. *J. Cell Sci.* **2005**, *118*, 5171–5180.
(21) DePinto, W.; Chu, X. J.; Yin, X.; Smith, M.; Packman, K.; Goelzer, P.; Lovey, A.; Chen, Y.; Qian, H.; Hamid, R.; Xiang, Q.; Tovar, C.; Blain, R.; Nevins, T.; Higgins, B.; Luistro, L.; Kolinsky, K.; Felix, B.; Hussain, S.; Heimbrook, D. In vitro and in vivo activity of R547: a potent and selective cyclin-dependent kinase inhibitor currently in phase I clinical trials. *Mol. Cancer Ther.* **2006**, *5*, 2644–2658.
(22) Wyatt, P. G.; Woodhead, A. J.; Berdini, V.; Boulstridge, J. A.; Carr, M. G.; Cross, D. M.; Davis, D. J.; Devine, L. A.; Early, T. R.; Feltell, R. E.; Lewis, E. J.; McMenamin, R. L.; Navarro, E. F.; O'Brien, M. A.; O'Reilly, M.; Reule, M.; Saxty, G.; Seavers, L. C.; Smith, D. M.; Squires, M. S.; Trewartha, G.; Walker, M. T.; Woolford, A. J. Identification of *N*-(4-piperidinyl)-4-(2,6-dichlorobenzoylamino)-1*H*-pyrazole-3-carboxamide (AT7519), a novel cyclin dependent kinase inhibitor using fragment-based X-ray crystallography and structure based drug design. *J. Med. Chem.* **2008**, *51*, 4986–4999.
(23) Dickson, M. A.; Schwartz, G. K. Development of cell-cycle inhibitors for cancer therapy. *Curr. Oncol.* **2009**, *16*, 36–43.
(24) Ali, S.; Heathcote, D. A.; Kroll, S. H.; Jogalekar, A. S.; Scheiper, B.; Patel, H.; Brackow, J.; Siwicka, A.; Fuchter, M. J.; Periyasamy, M.; Tolhurst, R. S.; Kanneganti, S. K.; Snyder, J. P.; Liotta, D. C.; Aboagye, E. O.; Barrett, A. G.; Coombes, R. C. The development of a selective cyclin-dependent kinase inhibitor that shows anti-tumor activity. *Cancer Res.* **2009**, *69*, 6208–6215.
(25) Parry, D.; Guzi, T.; Shanahan, F.; Davis, N.; Prabhavalkar, D.; Wiswell, D.; Seghezzi, W.; Paruch, K.; Dwyer, M. P.; Doll, R.; Nomeir, A.; Windsor, W.; Fischmann, T.; Wang, Y.; Oft, M.; Chen, T.; Kirschmeier, P.; Lees, E. M. Dinaciclib (SCH 727965), a novel and potent cyclin-dependent kinase inhibitor. *Mol. Cancer Ther.* **2010**, *9*, 2344–2353.
(26) Raynaud, F. I.; Whittaker, S. R.; Fischer, P. M.; McClue, S.; Walton, M. I.; Barrie, S. E.; Garrett, M. D.; Rogers, P.; Clarke, S. J.; Kelland, L. R.; Valenti, M.; Brunton, L.; Eccles, S.; Lane, D. P.; Workman, P. In vitro and in vivo pharmacokinetic-pharmacodynamic relationships for the trisubstituted aminopurine cyclin-dependent kinase inhibitors olomoucine, bohemine and CYC202. *Clin. Cancer Res.* **2005**, *11*, 4875–4887.
(27) Gao, Y.; Sharpless, K. B. Vicinal diol cyclic sulfates. Like epoxides only more reactive. *J. Am. Chem. Soc.* **1988**, *110*, 7538–7539.
(28) Calderón, F.; Doyagüez, E. G.; Fernández-Mayoralas, A. Synthesis of Azasugars through a Proline-Catalyzed Reaction. *J. Org. Chem.* **2006**, *71*, 6258.
(29) Kollonitsch, J.; Fuchs, O.; Gabor, V. New and known complex borohydrides and some of their applications in organic syntheses. *Nature* **1954**, *173*, 125–126.
(30) De Azevedo, W. F.; Leclerc, S.; Meijer, L.; Havlicek, L.; Strnad, M.; Kim, S. H. Inhibition of cyclin-dependent kinases by purine analogues: crystal structure of human cdk2 complexed with roscovitine. *Eur. J. Biochem.* **1997**, *243*, 518–526.
(31) Tetsu, O.; McCormick, F. Proliferation of cancer cells despite CDK2 inhibition. *Cancer Cell* **2003**, *3*, 233–245.
(32) Genovese, C.; Trani, D.; Caputi, M.; Claudio, P. P. Cell cycle control and beyond: emerging roles for the retinoblastoma gene family. *Oncogene* **2006**, *25*, 5201–5209.
(33) Giacinti, C.; Giordano, A. RB and cell cycle progression. *Oncogene* **2006**, *25*, 5220–5227.
(34) Zarkowska, T.; Mittnacht, S. Differential phosphorylation of the retinoblastoma protein by G1/S cyclin-dependent kinases. *J. Biol. Chem.* **1997**, *272*, 12738–12746.
(35) Takaki, T.; Fukasawa, K.; Suzuki-Takahashi, I.; Semba, K.; Kitagawa, M.; Taya, Y.; Hirai, H. Preferences for phosphorylation sites in the retinoblastoma protein of D-type cyclin-dependent kinases, Cdk4 and Cdk6, in vitro. *J. Biochem.* **2005**, *137*, 381–386.
(36) Campbell, A. D.; Raynham, T. M.; Taylor, R. J. K. Pyrazolopyrimidine compounds and their use in medicine. *Synthesis* **1998**, *1998*, 1707−1709.
(37) Chen, D.; Riedl, T.; Washbrook, E.; Pace, P. E.; Coombes, R. C.; Egly, J. M.; Ali, S. Activation of estrogen receptor alpha by S118 phosphorylation involves a ligand-dependent interaction with TFIIH and participation of CDK7. *Mol. Cell* **2000**, *6*, 127–137.
(38) McNae, I. W.; Kan, D.; Kontipidis, G.; Patterson, A.; Taylor, P.; Worrall, L.; Walkinshaw, M. D. Studying protein−ligand interactions using protein crystallography. *Crystallogr. Rev.* **2005**, *11*, 61–71.
(39) Lebedev, A. A.; Vagin, A. A.; Murshudov, G. N. Model preparation in MOLREP and examples of model improvement using X-ray data. *Acta Crystallogr., Sect. D: Biol. Crystallogr.* **2008**, *64*, 33–39.
(40) Zwart, P. H.; Langer, G. G.; Lamzin, V. S. Modelling bound ligands in protein crystal structures. *Acta Crystallogr., Sect. D: Biol. Crystallogr.* **2004**, *60*, 2230–2239.
(41) Vagin, A. A.; Steiner, R. A.; Lebedev, A. A.; Potterton, L.; McNicholas, S.; Long, F.; Murshudov, G. N. REFMAC5 dictionary: organization of prior chemical knowledge and guidelines for its use. *Acta Crystallogr., Sect. D: Biol. Crystallogr.* **2004**, *60*, 2184–2195.
(42) Skehan, P.; Storeng, R.; Scudiero, D.; Monks, A.; McMahon, J.; Vistica, D.; Warren, J. T.; Bokesch, H.; Kenney, S.; Boyd, M. R. New colorimetric cytotoxicity assay for anticancer-drug screening. *J. Natl. Cancer Inst.* **1990**, *82*, 1107–1112.
(43) Lopez-Garcia, J.; Periyasamy, M.; Thomas, R. S.; Christian, M.; Leao, M.; Jat, P.; Kindle, K. B.; Heery, D. M.; Parker, M. G.; Buluwela, L.; Kamalati, T.; Ali, S. ZNF366 is an estrogen receptor corepressor that acts through CtBP and histone deacetylases. *Nucleic Acids Res.* **2006**, *34*, 6126–6136.
(44) Workman, P.; Balmain, A.; Hickman, J. A.; McNally, N. J.; Rohas, A. M.; Mitchison, N. A.; Pierrepoint, C. G.; Raymond, R.; Rowlatt, C.; Stephens, T. C.; Wallace, J.; Straughan, D. W. UKCCCR guidelines for the welfare of animals in experimental neoplasia. *Lab. Anim.* **1988**, *22*, 195–201.
(45) Banker, M. J.; Clark, T. H.; Williams, J. A. Development and validation of a 96-well equilibrium dialysis apparatus for measuring plasma protein binding. *J. Pharm. Sci.* **2003**, *92*, 967–974.
(46) Gres, M. C.; Julian, B.; Bourrie, M.; Meunier, V.; Roques, C.; Berger, M.; Boulenc, X.; Berger, Y.; Fabre, G. Correlation between oral drug absorption in humans, and apparent drug permeability in TC-7 cells, a human epithelial intestinal cell line: comparison with the parental Caco-2 cell line. *Pharm. Res.* **1998**, *15*, 726–733.
(47) Kuhnz, W.; Gieschen, H. Predicting the oral bioavailability of 19-nortestosterone progestins in vivo from their metabolic stability in human liver microsomal preparations in vitro. *Drug Metab. Dispos.* **1998**, *26*, 1120–1127.
(48) Lipinski, C. A.; Lombardo, F.; Dominy, B. W.; Feeney, P. J. Experimental and computational approaches to estimate solubility and permeability in drug discovery and development settings. *Adv. Drug Deliv. Rev.* **2001**, *46*, 3–26.

(49) Sarwar, N.; Kim, J. S.; Jiang, J.; Peston, D.; Sinnett, H. D.; Madden, P.; Gee, J. M.; Nicholson, R. I.; Lykkesfeldt, A. E.; Shousha, S.; Coombes, R. C.; Ali, S. Phosphorylation of ER-{alpha} at serine 118 in primary breast cancer and in tamoxifen-resistant tumours is indicative of a complex role for ER{alpha} phosphorylation in breast cancer progression. *Endocr.-Relat. Cancer* **2006**, *13*, 851–861.

(50) Liscovitch, M.; Ravid, D. A case study in misidentification of cancer cell lines: MCF-7/AdrR cells (re-designated NCI/ADR-RES) are derived from OVCAR-8 human ovarian carcinoma cells. *Cancer Lett.* **2007**, *245*, 350–352.

(51) Parratt, M.; Bower, J. F.; Williamson, D.; Cansfield, A. Pyrazolo-pyrimidine compounds and their use in medicine. Patent WO2004/087707A1, 2004.